Évaluation biologique de métaux biodégradables pour une application de stent urétéral

Mémoire

Devi Paramitha

Maîtrise en génie des matériaux et de la métallurgie - avec mémoire
Maître ès sciences (M. Sc.)

Québec, Canada

Évaluation biologique de métaux biodégradables pour une application de stent urétéral

Mémoire

Devi Paramitha

Sous la direction de :

Hendra Hermawan, directeur de recherche

Stéphane Bolduc, codirecteur de recherche

Résumé

L'utilisation de stents urétéraux (endoprothèses urétérales) pour soulager l'obstruction des voies urinaires est toujours entravée par le problème de l'infection, de l'incrustation et de la compression, qui nécessitent une procédure de retrait. Un nouveau type de stents urétéraux biodégradables en matériaux polymères a été proposé pour surmonter ces problèmes. Des travaux récents ont proposé des métaux biodégradables à base de magnésium, comme nouveaux matériaux offrant à la fois résistance et biodégradation. Ce travail propose des alliages à base de zinc dont la cytocompatibilité avec les cellules urothéliales humaines normales a été évaluée par des tests 2D et 3D. Pour ce faire, les cellules ont été exposées à différentes concentrations d'extraits de métaux, 15 mg/ml de ZM21, 10 mg/ml de Zn-1Mg et 8,75 mg/ml de Zn-0,5Al. La mort cellulaire a été observée après 24 h, quoique en proportion différente pour chaque métal. Des modifications du cytosquelette des cellules a également été observée par immunofluorescence contre les cytokératines cependant, un processus de récupération des cellules a été noté au jour 3. La toxicité directe sur les cellules a été évaluée sur une construction de tissu urétéral 3D non tubulaire. Le résultat a montré que les cellules urothéliales pouvaient former un urothelium présentant des couches similaire à un tissu natif. Les protéines telles que la jonction serrée ZO-1 au niveau des couches superficielles et la laminine au niveau de la lame basale montre que le tissu reste sain au voisinage des disques métalliques après 7 jours de traitement. L'observation par MEB a montré que les cellules basales étaient attachées à la surface des métaux et observées dans un état d'étalement naturel, montrant que les pseudopodes et la morphologie fusiforme indiquent que les échantillons de métal sont non toxiques.

Abstract

The use of ureteral stents to relieve urinary tract obstruction is still challenged by the problem of infection, encrustation and compression leading to the need for removal procedure. A new type of biodegradable ureteral stents made of polymeric materials has been proposed to overcome the problems. Recent works proposed magnesium-based biodegradable metals as new materials offering both biodegradation and strength. This work proposes zinc-based alloys by firstly evaluating their cytocompatibility toward normal human urothelial cells using 2D and 3D assays. Cells were exposed by different concentration of metals extracts, 15 mg/ml of ZM21, 10 mg/ml of Zn-1Mg and 8.75 mg/ml of Zn-0.5Al. Induction of cell death was observed after 24 h, resulting in reduced cell viability at different percentages for each metal. The cytoskeleton of cells was also affected as observed by immunofluorescence of cytokeratins however, the recovery process of cells was noted at day 3. Direct cell toxicity was evaluated on a non-tubular 3D ureteral tissue construct. The results showed that urothelial cells could form a multilayered urothelium as in a native tissue, with the presence of tight junction ZO-1 in superficial layer and laminin in the basal layer indicating that the tissue is healthy in the presence of the metal disks even after 7 days of treatment. SEM observation showed basal cells were found attached to the metal surface and seen as in a natural spreading state, showing pseudopodia and fusiform morphology indicating that the metal specimens are non-toxic.

TABLE OF CONTENTS

LIST OF TABLES

LIST OF FIGURES

LIST OF EQUATIONS

LIST OF ABBREVIATIONS

Al	Aluminum
ASTM	American Society of Testing Materials
aU	Artificial Urine
AUS	Allium Ureteral Stent
BM	Biodegradable Metal
FBS	Fetal Bovine Serum
FDA	Food and Drug Administration
Fe	Ferrum/Iron
IC_{50}	Inhibitory Concentration 50
ICP/MS	Inductively Coupled Plasma Mass Spectrometry
ISO	International Organization for Standardization
Mg	Magnesium
MTT	3-(4,5-Dimethylthiazol-2-Yl)-2,5-Diphenyltetrazolium Bromide
NaCl	Sodium Chloride
NHUCs	Normal Human Urothelial Cells
PBS	Phosphate Buffered Saline
SEM	Scanning Electron Microscopy
UC	Urothelial Cell
UE	Ureteral Equivalent
US	Ureteral Stent
USP	United States Pharmacopeia
UTI	Urinary Tract Infection
UV	Ultra Violet
WST	Water Soluble Tetrazolium
Zn	Zinc

Acknowledgement

The completion of this project was not possible without the contribution of each and every one who was involved in many different ways and thus I would like to dedicate this page to them. First of all, I would like to express my gratitude to my research director, Hendra Hermawan, for his patience, his availability and for giving me the opportunity to continue my studies and involve in such a challenging project. To my co-director Stéphane Bolduc, I am very grateful for putting so much efforts and expertise on this project.

I would like to thank Stéphane Chabaud who trained and provided me with guidance, help, expertise, and never-ending problem solving during the completion of my project.

I would also like to thank Ehsan Mostaed and Maurizio Vedani from Politecnico di Milano, Italy for providing us with the metals they have developed in their laboratory.

I would like to thank the other members of the research team: Reza, Sébastien, and Adji.

I would also like to thank my professor in Indonesia, Deni Noviana who gave me the opportunity to be involved in research and clinical practice, and for his invaluable moral support. Many thanks also to M. Fakhrul Ulum and Leni Maylina for their guidance and support.

I would like to thank my bestfriend, my roommate, my sister: Imene for her generosity, moral and infinity support. I would also like to thank Agung for his encouragement, emotional and intellectual support. To Rhani and Ian, who have provided the time to read and proofread this manuscript in the midst of their busy life, also for their support and laughter. To my family in Montréal, my second parents: mbak Menuk and Pak Endro, I would like to thank for their huge support, warmness and positivity that they offered at any time.

Finally, I would like to warmly thank my parents, my sisters Handiny and Dhania, my brothers Fahmi and Rian, my niece Khaleyla, and my nephew El Fatih. I would like to let them know that I could not have finished without them.

Chapter 1 Literature Review

1.1 The urinary system

1.1.1 Kidneys

Urinary system, also known as renal system, has an important role in maintaining homeostatic condition by filtering and excreting waste products from our body. This system is divided into upper and lower tracts (Figure 1). Upper tract consists of kidneys which filter waste from the circulating blood into the urine. Ureter connects the upper with the first part of lower urinary tract, the bladder, where the urine is stored. Urethra and striated sphincter are the following organs in the lower tract [1].

There are two kidneys in the human body, located in the posterior abdomen wall. Kidney of the adult human weighs around 150 grams. Kidneys have delicate structures and on the outer, are covered by a tough fibrous capsule as a protection. Hilum is a region in the medial part of kidneys where the artery and vein, lymphatics, nerve supply, and ureter pass. Inner part of the kidney is divided into outer cortex and inner region medulla (Figure 1). The kidneys receive blood flow representing 22 percent of the cardiac output equal to 1100 ml/min. The blood enters kidney through the hilum, where renal artery which carries blood then divided into smaller branch arteries. These arteries lead to the glomerular capillaries that filters large amounts of fluid and solutes and start the urine formation [2].

The function of the kidney generally is to filtrate the blood, but it also performs important functions i.e. maintaining body fluid balance, regulating minerals in human body by filtering them from the blood, waste materials, and also producing hormones that are involved in red blood cells production, promoting bone health, and blood pressure regulation. The function of the kidney is derived from its functional unit, the nephrons, as many as 1 million per kidney. Each nephron is capable of forming urine. Nephron cannot be regenerated by the kidney, therefore there is a gradual decrease of their number following kidney injury, disease, or normal aging [2].

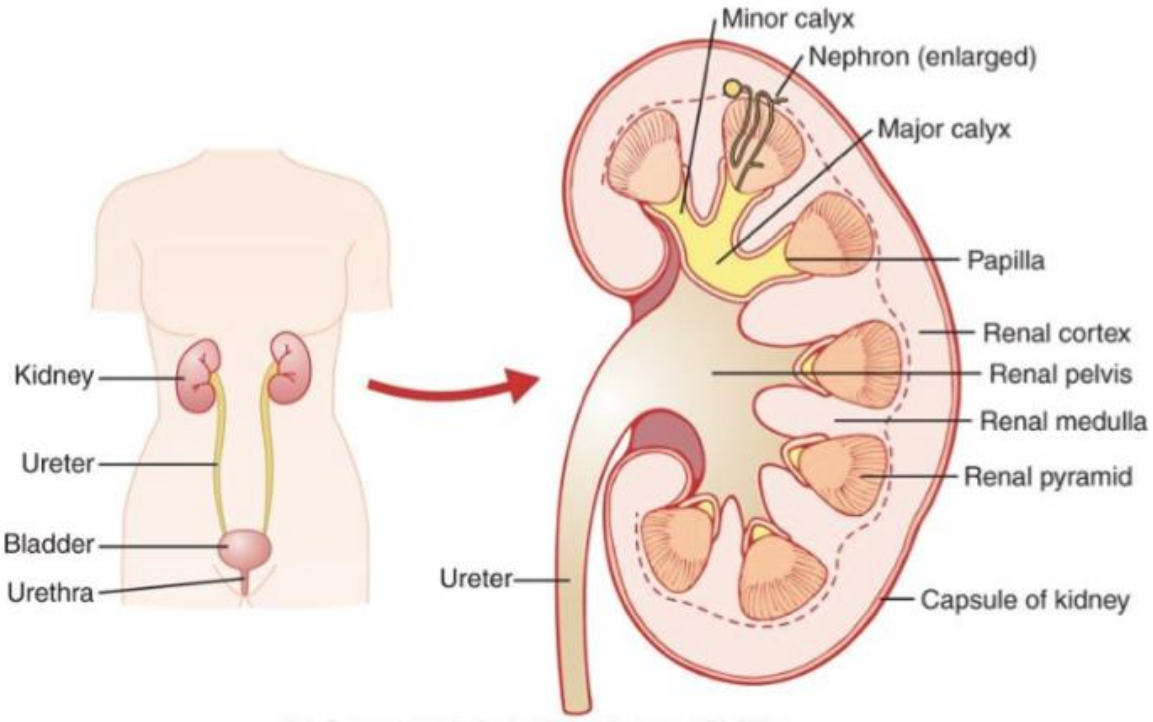

Figure 1 The scheme of normal urinary system anatomy (left) and kidney longitudinal section (right) [2].

1.1.2 Urine

The urine produced in the renal parenchyma is then collected in the renal pelvis of the kidney with its funnel-shaped and passes through the ureter, 25-30 mm long tubes with an outer diameter of 4-5 mm in adults and stored in the bladder [3, 4]. Ureteral peristaltic is the rhythmic coordinated contractions pushing urine down to the bladder at flowrates 0.5-10 ml/min for each kidney/ureter. Bladder stores urine at low pressure until micturition occurs, and during the voiding, the pressure of the bladder rises, pushes urine flow to the urethra, sphincter and out of the body. The average volume of urine released in each voiding is about 300 ml, in approximately 40 seconds for 6 times a day without any leakage, in a healthy system [3, 5].

Kidneys have the ability to concentrate urine, which determines how much urine volume to be excreted every day to remove ingested ions and waste product from body metabolism. The concentration of urine should be more than plasma fluids and the maximum

concentration in normal condition is 1200-1400 mOsm/L, four to five times higher than plasma. When one consumes excess water, the kidney can excrete dilute urine as much as 20 L per day with concentration as low as 50 mOsm/L. In case of deficit water, concentrated urine is formed and continue to excrete solutes while increasing water reabsorption and decreasing the volume of urine [2].

The urine pH ranges widely from 4.5 to 8.0, depending on the body acid-base equilibrium state. Generally, on a regular average diet the pH ranges from 5.0 to 6.5. Urine pH mainly depends on the bicarbonate (HCO_3^-) concentration in the blood, the higher the ion concentration the higher the pH. On the contrary, the reduction of pCO_2 in the blood causes a sharp increase in urine pH [6].

Urine is composed by various substances in different concentrations. The substances are inorganic cations (sodium, potassium, ammonium, calcium, and magnesium) and anions (chloride, sulphate, and phosphate) and organic components such as urate, creatinine, oxalate, and citrate. Urine composition is strongly related to stone formation. Table 1 provides the complete human urine components. Urine biochemical analysis provides information for medical examination, and a conclusion can be given in laboratory based on this data, pH level, and urine density. The other required information are the registration of sex, age, and diuresis [7].

Table 1 An analog representing the composition of typical human urine [8].

Component		Amount (mg/L)
Inorganic salts:		**14.157**
	Sodium chloride	8.001
	Potassium chloride	1.641
	Potassium sulfate	2.632
	Magnesium sulfate	783
	Magnesium carbonate	143
	Potassium bicarbonate	661
	Potassium phosphate	234
	Calcium phosphate	62
Urea		**13.400**
Organic compounds:		**5.369**
	Creatinine	1.504
	Uropepsin (as tyrosine)	381
	Creatine	373
	Glycine	315
	Phenol	292
	Histidine	233
	Androsterone	174
	1-Methylhistidine	173
	Imidazole	143
	Glucose	156
	Taurine	138
	Cystine	96
	Citrulline	88
	Aminoisobutyric acid	84
	Threonine	83
	Lysine	73
	Incloxysulfuric acid	77
	m-Hydroxyhippuric acid	70
	p-Hydroxyphenil-hydrocrylic acid	70
	Inositol	70
	Urobilin	63
	Tyrosine	54
	Asparagine	53
	Organic less than 50 mg/L	606
Organic ammonium salts:		**4.131**
	Ammonium:	
	Hippurate	1.250
	Citrate	756
	Glucoronate	663
	Urate	518
	Lactate	394
	L-Glutamate	246
	Aspartate	135
	Formate	88
	Pyruvate	44
	Oxalate	37
	Total solutes	**37.057**

1.1.3 The ducts: urothelial cells

Urinary tract mucosa is lined by epithelial cells called urothelial cells. They form layers of cells known as urothelium or uroepithelium (Figure 2). This epithelium lines the urinary tract from the renal pelvis of kidneys to the base of urethra. Urothelial cells are highly-specialized transitional epithelial cell. Depending on their differentiation state, the three kinds of urothelial cells are called basal or stem cell, intermediate, and superficial cells. Basal cells have a size of approximately ~10 μm and lay on a single layer on the basal membrane and form intimate contacts with capillary bed. Intermediate cells, pear-shaped or pyriform, form 1-5 layers with cell diameters ranging from 10-15 μm. These cells play an important role when there is a damage that causes loss or removal of superficial cells. Intermediate cells then differentiate into superficial cells rapidly. Superficial cells cover the luminal surface of the urinary tract with their long axes parallel to the basal lamina. The so-called umbrella cells are polyhedral shape (typically sided 5-6), 25-250 μm in width, having mono or multinuclei depending on the species. Unlike other epithelial cells that have high turnover rates as the intestine or skin (1.5-30 days), urothelial has turnover rates of ~3-6 months. But their tremendous regenerative capability could be seen in the event of damage, the lost cells are replaced quickly within days of significant damage [9, 10].

Urothelium main role is to be a barrier against ion, solute and water flow. This function is related to a particularly high transepithelial resistance of urothelium (20,000 to >75,000 $\Omega \cdot cm^2$). In addition, other functions of urothelium as the first line of contact with urinary environment, the layers of cell have the capability of sensing the changes within the lumen, both chemical and mechanical. Urothelium then release prostaglandins, chatecholamines and cytokines as signals to smooth muscle, neurons and capillaries [9].

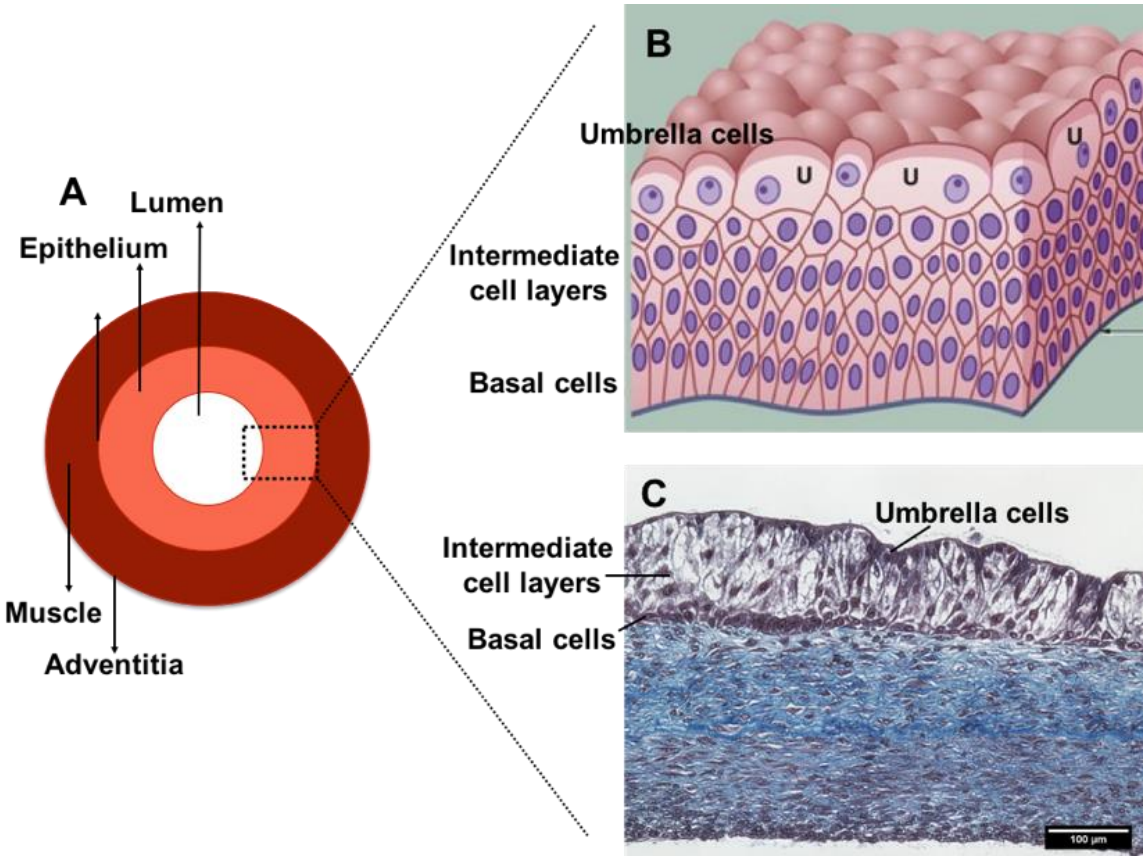

Figure 2 (A) Schematic transverse section of ureter, B) urothelium [11], and C) histological transverse section of tissue-engineered ureter with Masson Trichrome staining.

1.2 Obstructive uropathy

The urinary system is susceptible to a variety of infection and other problems, such as blockage and injuries. Obstruction of the urinary tract or obstructive uropathy can occur at any portion of the system, both single and multiple levels. Obstructive uropathy is known to be the most identifiable cause of renal insufficiency and failure in infants and children [1, 12].

The most notable effect of obstructive uropathy is the occurrence of hydronephrosis as the manifestation of flow blockage. The damage of renal parenchymal will occur following hydronephrosis. Renal parenchyma consists of three compartments that is cortex, medulla, and interstitium. Each compartment is responsible for tasks, which are very important to the body: from blood filtration, maintaining body homeostasis until reabsorption of ions and

minerals. Damaged renal parenchyma means kidney failure and affects the other organ system in the body as compensation. Cardiovascular system failure will occur and it leads to liver failure [1, 13]. As mentioned by Reyner et al, the mortality and morbidity are significantly higher in patients with obstruction [13].

Urinary tract obstruction can be divided into upper and lower tract obstruction, depending on the affected location. Upper urinary tract obstruction is found frequently in urology, with lifetime incidence is 12% in men and 6% in women [5]. The most common cause of acute and chronic upper tract obstruction is due to calculus or stones; however, in lower tract, especially in men most cases are due to benign prostatic enlargement. Based on the cause, it can be intrinsic or extrinsic and physiological or pathological (Table 2).

The obstruction can be acute or chronic. In chronic obstruction especially the one located in the ureter can be occurred by either intra- or extraluminal causes. The intraluminal causes are calculi/stones, stricture, ureteric valves, tuberculosis, transitional cell carcinoma or ureteritis cystica. The extraluminal causes can be physiological such as pregnancy or pathological, such as ureterocele, retrocaval ureter, aortic aneurysm, radiation, retroperitoneal fibrosis, para-aortic lymph nodes, iatrogenic or intra-abdominal malignancy [5].

Table 2 Etiology of obstructive uropathy [4].

Congenital		Acquired	
Intraluminal	Extraluminal	Intraluminal	Extraluminal
PUJ obstruction	Bladder diverticulum	Calculus	Malignancy (pelvic: prostate, colorectal, ovarian, uterine, cervical; retroperitoneal: lymphoma, sarcoma, mesothelioma, metastases)
Ureteric atresia	Vascular (retrocaval ureter, retroiliac ureter, lower pole renal vessels, persistent umbilical artery)	Stricture	Gastrointestinal (pancreatitis, appendicitis, diverticulitis, Crohn's disease)
Ureteric valve		Urothelial tumor	Vascular (abdominal aortic aneurysm, iliac artery aneurysm)
Ureteric folds		Blood clot	Pregnancy
Congenital stricture		Sloughed papilla	Gynaecological (fibrosis, endometriosis)
Vesicoureteric reflux		Benign polyp	Retroperitoneal fibrosis
Primary megaureter		Foreign body (stent)	
VUJ obstruction		Fungal ball	
Ureterocele (ectopic, orthopic)			

1.2.1 Ureteral obstruction

Ureteral obstruction or blockage generally caused by extrinsic, intrinsic, and intraluminal factors (Figure 3). The obstruction can be partial or developing progressively into complete obstruction. Unilateral ureteral obstruction is more frequent than bilateral obstruction and it can be in the proximal, middle or distal part of ureter. Extrinsic causes are usually compression on the ureter caused by physiological changes or pathological disorders of surrounding organs, including retroperitoneal fibrosis, obstetric and gynecologic causes in women (pregnancy, tumor, abscess or lesions on retroperitoneal part of uterus or ovary), and vascular causes, such as aneurysm of abdominal aorta and iliac artery and compression from vascular graft. Intrinsic causes involve the ureteral wall, including fibrosis, stricture, abscess, tumor of ureteral wall and foreign body with granulomatous reaction (submucosal stone). Intraluminal causes are usually ureteral calculus/stones, blood clot or necrotic debris, and inflammatory mass lesions [4].

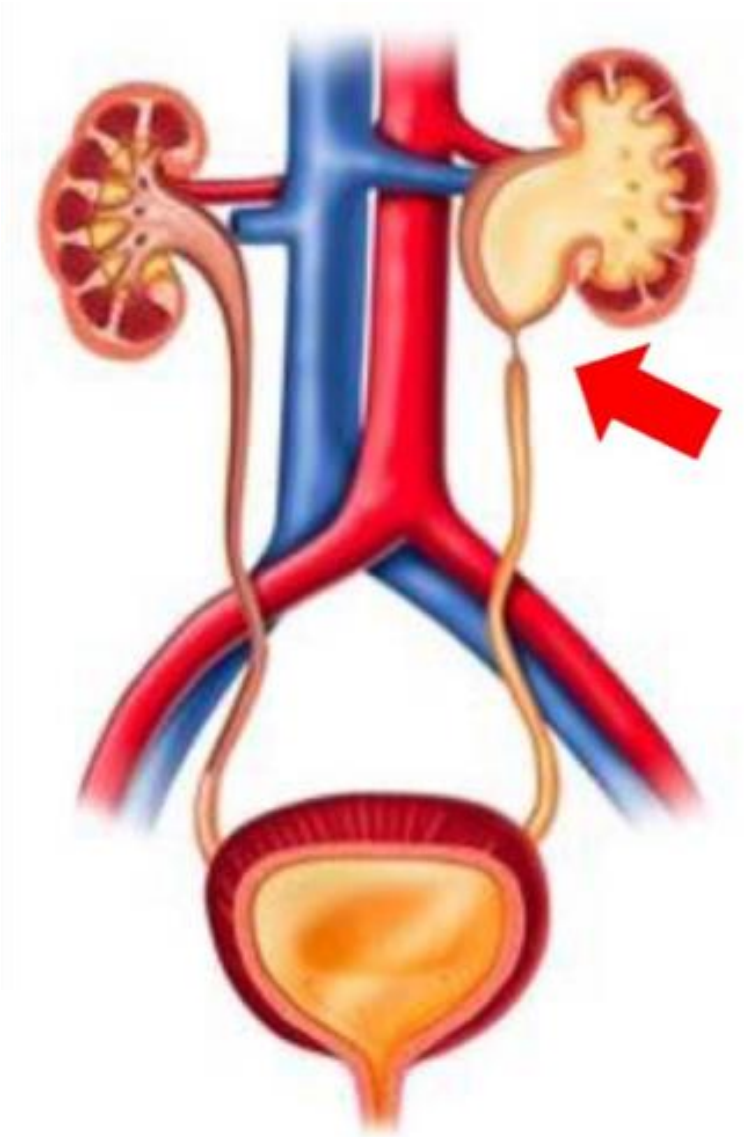

Figure 3 Illustration of an obstructed ureter at the uretero-pelvic junction [14].

The effect of ureteral obstruction on the kidney is a major concern. As stated by Gulmi & Felsen [4], when obstruction occurs, in the first hours the ureteral pressure and renal blood flow change caused by the dilation and constriction of afferent and efferent arterioles in the kidney. This change in normal physiology will cause the inability of the kidney to concentrate the urine even after the obstruction is removed. This means that there is defect in the glomerulus, the functional unit of kidney. In bilateral ureteral obstruction, the events happen faster. Colicky flank pain is characteristic of acute unilateral ureteral obstruction, with the presence of fever suggestive of infection.

1.2.2 Treatment for urinary obstruction

The obstruction however should be removed to avoid greater damage to the body system. Numerous therapeutic options are available, but the treatments are depending on several factors. The factors such as comorbidities, age, prior surgery, compliance of the patient, and the surgeon's skill, which also need to be familiar with various techniques. Intrinsic obstruction, especially when it is short, i.e. ~2 cm, is considered more manageable through endourological procedures. Extrinsic obstructions are usually longer than intrinsic causes and require more invasive repairs or long-term stents can be a choice. The removal of obstruction can be performed by using antegrade, retrograde or laparoscopic surgical approaches. Laparoscopy is usually done in the case of pyeloplasty for ureteropelvic junction obstruction, ureteroureterostomy for midureteral strictures, or ureteral reimplant for a distal stricture [15].

In some cases, the surgery cannot be done and regardless of the treatment selected, a stent implantation will be required at some point in majority of cases. The stent implantation can be temporary or permanent, depending on the etiology of the obstruction. Ureteral stent is an indwelling tubular device that resides in the kidney, ureter, and bladder containing means for retaining ends of tube in kidney and bladder. It facilitates the urine to flow in blocked or wounded ureter from the kidney to bladder and has been used since 1970s [3, 16, 17].

1.2.3 Ureteral stent for ureteral obstruction

The reason for ureteral stent utilization can be to provide a scaffold for healing after endoureterotomy, to maintain the flow of urine in chronic obstruction, and as a prophylactic measure to guard against the ureteral obstruction development. The third reason usually follows treatments such as ureteroscopy, ureteroneocystostomy, ureteroureterostomy, or ureteroenteric anastomosis. The etiology of stent placement can be divided into intrinsic and extrinsic causes. Intrinsic obstruction such as iatrogenic, infection from tuberculosis, inflammation caused by ureteral stones, and ureteropelvic junction obstruction, which is

congenital. Extrinsic obstructions are caused by metastatic tumor disease, radiation and retroperitoneal fibrosis [18].

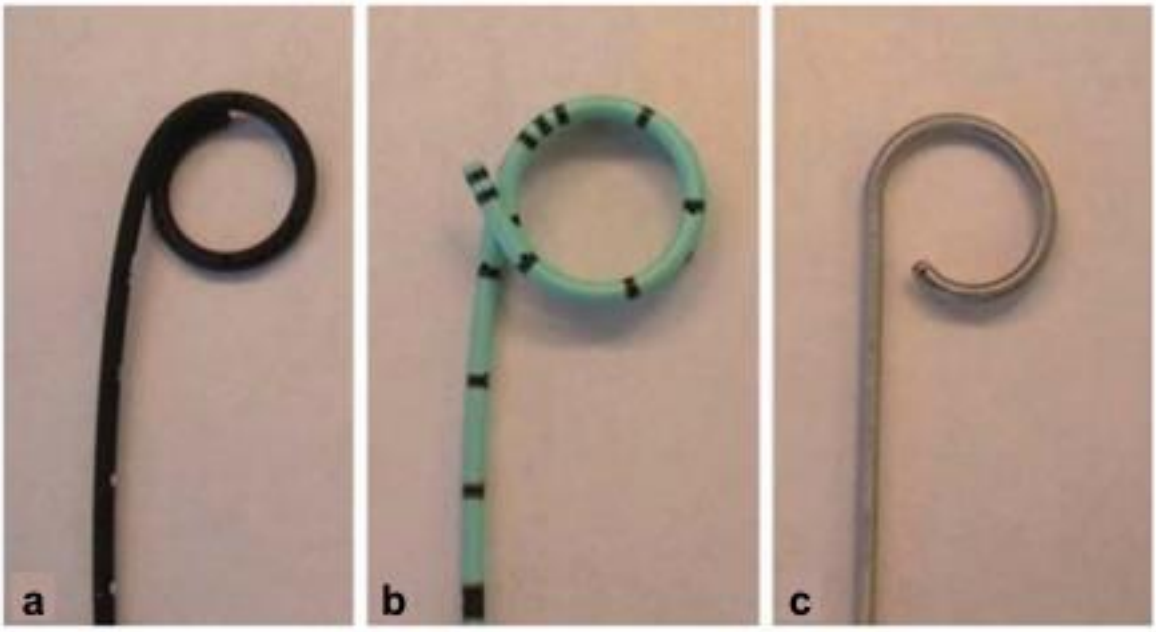

Figure 4 Representative double-J stents. a, Silicone; b, Polyurethane; c, Metal (Resonance) [15].

The placement of a stent is not without problem. Stent inside the urinary tract can induce irritation and bleeding of mucosal membrane due to the friction with the stent then blood in the urine, or hematuria, occurs. The junction between bladder and urethra that is usually closed, is kept open with the presence of stent and raise the possibility of infection. In long term use, precipitation of salts in the urine leads to crystalline deposits on the stent surface. The build-up deposits or encrustation will eventually play a role in further blockage, if it is severe, the removal will be difficult and painful. Ureteral stent is associated with high morbidity in up to 80% of patients; and the most common side effects are pain in the flank region, hematuria, irritative voiding symptoms and reduced working time [3].

Urinary stents are divided into 2 types: indwelling and external. Modern stents nowadays have retention coils and shape memory, which helps to prevent stent from moving or migrate. Basic designs of stent are pigtail, J-stent, cross-coil, and double pigtail/double-J.

The most popular design that is used today is the double-J stent (Figure 4). Stent duration should be determined because the risk of infection and encrustation is greater along with the dwelling time. The determination of stent indwelling time must be the balance of two objectives: 1) allowing the stent to act as a scaffold to facilitate healing following treatment of obstruction, 2) avoiding infection and inflammation which lead to fibrosis. Prolonged duration of stenting increases risk of infection as well as inflammation, this may result in fibrosis and restructuring which risk increases over time [15]. No perfect stent has been found up until now, but the ideal stent should be strong to keep the lumen opening; antibacterial, so that the bacterial cannot or reduce the ability of it to multiply themselves inside the biofilm; could avoid calcification on its surface, thus the possibility of encrustation is less to occur. Another aspect that is desirable is the elimination of removal surgery, which reduce both the morbidity and the overall costs [3].

1.2.3.1 Current ureteral stents technology

The development of urinary stent is continuously ongoing. The available stents can be grouped into 4: plastic polymeric, coated, drug-eluting, and metal stents (Figure 4). Polymeric stents are usually made of silicone which is the current gold standard for ureteral stents. It is highly compatible with tissue and resistant to encrustation, but the extreme flexibility of this material brings the difficulty of stent passaging. Polyurethane is also flexible but more rigid than silicone, yet it is found to cause more urothelial erosion and ulceration than other materials. It may also induce cytotoxic reaction from its degradation products accumulated and left for extended periods of time. The other polymeric stents are made of polyurethane and the combinations of those mentioned before. Several proprietary biomaterials have also been developed with the goal of retaining the flexibility and inert nature of silicone but with more rigidity: Silitek (Surgitek, Racine, WI, USA), C-Flex (Consolidated Polymer Technologies, Clearwater, FL, USA), and Percuflex (Boston Scientific, Natick, MA, USA) [15, 19].

Stents coated with chemical, another material or proteins are usually used to prevent bacterial adhesion which leads to infection and encrustation. The coating prevents bacteria or mineral deposits to adhere on the stent surface. Heparin, diamond-like carbon, silver,

antimicrobial peptides and marine mussel proteins are the examples of coating material. Hydrogels are also used to coat stents, which provide improved biocompatibility by reducing irritation and cell adhesion. Prevention of infection can be done by inhibiting the growth of bacteria. Some stents are coated with drugs to have this efficacy, namely triclosan, combination of antimicrobial peptides and antibiotics, also combination of anti-proliferative drugs with antibiotics. Ketorolac, an NSAID drug that has been used in local post-operative treatment of urinary tract is also used to coat stent to decrease inflammation and hyperplasia [15, 20]. Lange et al. [21] reported their results of in-vitro antibacterial activity studies on heparin-coated (Resonance, Cook Medical) and triclosan-eluting (Triumph®, Boston Scientific) commercial stents. Bacterial strains used were *Escherichia coli, Enterococcus faecalis, Klebsiella pneumonia, Staphylococcus aureus,* and *Pseudomonas aeruginosa.* Experiments were conducted in a simulated urinary condition. The result showed that triclosan was more effective than heparin in preventing the adhesion and multiplication of bacteria, as well as biofilm formation.

A recent study by Wang et al. [22] used controllable and sustained release silver as coating on polydopamine pre-treated silicone urinary catheter. Their study has shown the efficacy of silver ions with reduced *E. coli* colonization and encrustation compared to a silver-coated Dover™ commercial catheter. Silver ions work in 2 ways: 1) bound with sulfur group in bacterial membrane which makes it permeable and render the bacteria susceptible to antimicrobial drugs, and 2) interfering with bacterial metabolism causing a higher production of reactive oxygen species (ROS). This leads to the damage inside the bacterial cells by harming the DNA, proteins and membrane, then bacteria will eventually lyse [23]. In addition, silver able to turn living bacteria into ‘zombie’ which kills the other living bacteria by carrying the silver ion inside their cell [24].

1.2.3.2 Metallic ureteral stent

Polymeric stents that are used to treat obstruction caused by malignancy demonstrated high failure rates up to 58%. Chronic obstructions, such as from external fibrosis or malignant tumor, are usually cases for which ureteral stent placement is recommended instead of

surgery. Those cases are poor operative candidates because surgery is more invasive than endoscopic stent placement. Polymeric stents with metal reinforcement, to give stronger opening against obstruction, are preferred. Metal stents demonstrated relative success to treat chronic obstruction compared to polymeric stents [15, 19].

Metal stents with inherent strength are used mostly to maintain lumen opening from tight ureteral compression, internally or externally. Various designs of short metal stent have been developed and used in clinical practice for over 15 years, yet none was found in the style of an indwelling ureteral stent. Concerns brought by metal stents include biocompatibility, hyperplastic tissue response and encrustation. On the other hand, the rigid metallic stent leads to bothersome lower urinary tract symptoms such as pain, discomfort, dysuria and gross hematuria. The problems lead to early removal and more procedures, i.e. change into polymeric stent, to treat the chronic obstruction [15, 19].

Available commercial metal ureteral stents are found on the market with different purposes (Figure 5). Those stents are made of mixture of metal-metal and metal-polymer. The Resonance® metal stent is a continuous unfenestrated metal coil with an inner safety wire welded to both closed, tapered ends. The material combination of nickel, cobalt-chromium and molybdenum provide an ultrahigh tensile strength and resistance to corrosion. Its flexibility and compatibility with magnetic resonance imaging are not only the advantages, this stent is also resistant to encrustation and no report of stent failure to date. One concern to the development of metallic ureteral stents is to improve the discomfort experienced by the patients. A more flexible stent that is already on the market, Passage® also known as Snake stent, is a metallic coil stent with increased flexibility and durable radial compression. This stent is less tight with opening at both ends, makes it more flexible and comfortable than Resonance® does. It is reported that Passage® stents have lower tensile strength and higher resistance to radial compression, which increased the comfort and better prevention to high compression caused by tumor ingrowth or stent compression, in the same time [19]. The summaries of metallic ureteral stents characteristics are presented in Table 3.

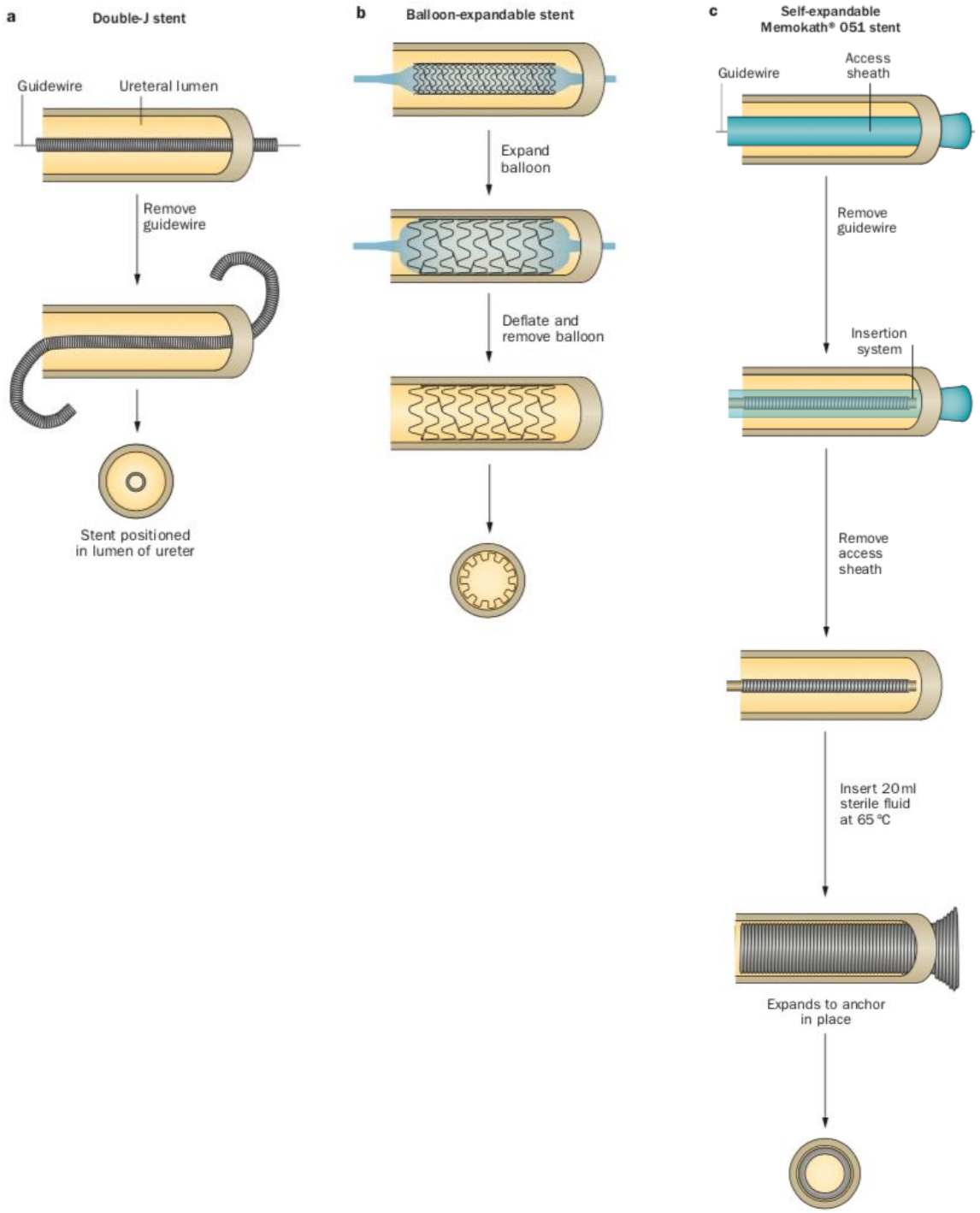
a
Double-J stent
Guidewire
Ureteral lumen
Remove guidewire
Stent positioned in lumen of ureter
b
Balloon-expandable stent
Expand balloon
Deflate and remove balloon
c
Self-expandable Memokath® 051 stent
Guidewire
Access sheath
Remove guidewire
Insertion system
Remove access sheath
Insert 20 ml sterile fluid at 65 °C
Expands to anchor in place

Figure 5 Appearance and insertion of metal stents studied for use in the ureter a, Double-J stent; b, Balloon-expandable stent; and c, Self-expandable Memokath® 051 stent [3].

1.2.3.3 Biodegradable metal ureteral stents

An ideal ureteral stent for the future is believed to be degradable, antibacterial, and would prevent mineral deposition. Development of urinary devices has been done continuously with regards to the material of the device or the coatings to have surface-changing properties. The development aims to prevent bacterial adhesion and infection. The changing surface in both physical and chemical properties prevents bacterial attachment and colonization as well as mineral deposits. In term of surface changing properties, degradable US are more likely to have advantage in this case. Another advantage of degradable US is that it does not need the removal surgery, which reduce the morbidity of patients and overall cost. Degradable US commercially available to date mostly made of polyurethane (Tecoflex®, APR Medtech; BARD®, Bard Medical). Other polymers used as ureteral stent materials have been reported such as polylactic acid (PLA), poly(glicolic acid) (PGA), and poly(lactic-co-glicolic acid) (PLGA) [25-30]. Those US have shown their biocompatibility and less in both inflammation and morbidity because of their softness. However, this softness and low tensile strength could provoke difficulties to keep the lumen open from extrinsic compression [31]. Therefore, metal-reinforced polymeric stent is available to meet the needs (Silhouette®, Cook Medical).

Metal stents are a good alternative to polymer stents to treat ureteral obstruction caused by external compression due to their inherent strength (Table 4). Metals that degrade safely in human body, biodegradable metal (BM), should be a good alternative. They will not only provide a structural strength, but also could avoid encrustations and bacterial adhesions because of their changing surface properties. Those stents could ameliorate patient

morbidity associated with secondary removal procedures or forgotten stents [19].

Table 3 Characteristic of current commercial metallic ureteral stents [19].

Name	Material	Structure	Deployment
Double-J stents			
Resonance® (Cook Medical, USA)	Nickel-cobalt-chromium-molybdenum alloy	Tightly coiled metal wire with conventional kidney and bladder curls that are occluded	Through 8 Fr outer sheath
Silhouette® (Applied Medical, USA)	Polyurethane and metal	Polymer stent reinforced by metal wire coiled	Guidewire and pusher
Passage® (Prosurg, USA)	Metal Gold-plated metal (Snake stent)	Spiral windings along a tubular coiled structure configured with flexible, curved pigtails	Guidewire and pusher
Self-expandable stents			
Memokath® 051	Nickel-titanium alloy	Bare metal stent with a closed spiral shape and a fluted end for anchoring	Thermo-expandable, introduced inside an access sheath
Allium® Ureteral Stent (Allium Medical, Israel)	Metal and polymer	Metal structure with self-radial-expanding design covered with a thin layer of polymeric material	10 Fr deployment device

Biodegradable metal has been studied and reported for urinary applications. A study conducted by Zhang et al. [32] investigated Mg-6Zn degradation and compatibility both *in vitro* and *in vivo* in bladder of rats. The results showed that the degradation rate of Mg-6Zn was higher than pure Mg and had no toxic effect on the bladder tissue after 2 weeks of implantation. Another study by Lock et al. [16] using pure magnesium (Mg) and Mg-based alloys (Mg-Ytrium, Mg-Al-Zn) co-cultured with *E. coli* for 3 days in aU solution, showed

that all the Mg samples showed mass loss, indicating the degradation has occurred as well as the commercial polyurethane stent as comparison. In addition, Mg samples had an antibacterial activity, the culture of bacteria with this metal resulting in a significant reduce viability.

Table 4 Mechanical properties of biodegradable materials [33].

Metal	Mechanical properties			Degradation rate (mm/year)
	YS (MPa)	UTS (MPa)	ε (%)	
SS316L	190	490	40	-
Mg-Al (AZ31, extruded)	175	250	14	2.0
Mg-1Zn (rolled)	160	240	7	1.52
Zn-1Mg (cast)	-	150	2	0.20
Zn-3Mg	205	220	6	0.28
Polymer PLLA	3-5	60-80	>50	N/A
Polymer PLGA	2-4	40-60	>50	N/A

Biodegradable metals that have been used or proposed for biomedical applications are magnesium (Mg), iron (Fe) and zinc (Zn). These metals are trace elements and found in human and animal's body. Hundreds of reports about Mg are available up until now regarding the characterization of the microstructures, testing of the mechanical properties, degradation behavior and ion release, and *in vitro* and *in vivo* biocompatibility studies to evaluate the feasibility of these Mg-based BMs for biomedical purposes [34]. Compared with Mg-based BMs, Fe-based BMs have similar mechanical properties as stainless steel and are more attractive from a structural point of view. However, the preliminary animal tests have revealed a slow degradation rate of pure iron *in vivo* [14]. Hence, research has focused on the development of new kinds of Fe-based BMs by modifying the chemical

composition, microstructure, and surface of Fe with diverse manufacturing process technologies [34]. Meanwhile, Zn and its alloys is an alternative for Mg and iron (Fe), because of their moderate degradation rate and its compatibility has been proved *in vitro* [35, 36] and *in vivo* [37, 38]. Zinc is a micronutrient and plays an important role in animals and humans, even in higher plants. It is involved in enzyme metabolism, DNA and gene expression [39]. It also has an antibacterial activity especially in the gut, even though the mechanism of action is still unclear [40-42].

1.3 Biological assessment of biodegradable metal for ureteral stent

Stents, as man-made medical devices, are regulated for interstate distribution by the Federal Food and Drug Administration (FDA) in The United States. Before those medical devices can be distributed and used, biocompatibility testing should be done. This regulation has been existing since 1976 in the United States, which called for the establishment of three classes of medical devices. Class 1 devices are those that present little or no risk to the user, Class 2 presenting some risk and Class 3 presenting a high degree of risk to the user. The European Union has a similar classification of medical devices and recognized as Medical Device Directive [43].

1.3.1 The need for biological assessment for stent materials

The term biocompatible for medical devices refers to the safety of use in the general population, and biocompatibility of a material can be defined as the materials used in a medical device do not elicit a reaction that either makes the device not perform its intended use, or causes reactions that affect the functioning and health of the host [43]. Biocompatibility testing in general is conducted to answer 2 questions, i.e. 1, the safety of materials and 2, whether it has the necessary physical and mechanical properties for the proposed function. Furthermore, elements which should be noted from the medical devices that will undergo biocompatibility testing are: 1) type of material, 2) end-use of the device, in other words, is it for medical use or not? 3) function of the material within the device, and 4) is there any available existing data on the material? [44].

Type of material is important because all materials used in medical devices trigger host response. The response could be immediate, prolonged or delayed after contact with the device. The outcome depends on several factors: site of implantation, host species and genetic makeup, implant sterility, and duration of implantation. Those are the parameters that should be considered for conducting a biocompatibility test [43].

An appropriate series of tests can be selected after determining the parameters mentioned above. These tests are usually done to identify the success or failure of the biomaterial implants and its intended application. *In vitro* and *in vivo* biocompatibility tests are necessary to evaluate both adverse and successful reactions of biomaterial implants. Identified adverse responses from tissue should be weighed together against the benefits of the biomaterial implants to be used, known as risk assessment evaluation. In this evaluation, additional tests should be done to give a rational reason and justification to continue using the biomaterials with the presence of the adverse responses [45]. The flowchart below explains the steps to determine whether biological evaluation or biocompatibility testing should be done or not (Figure 6).

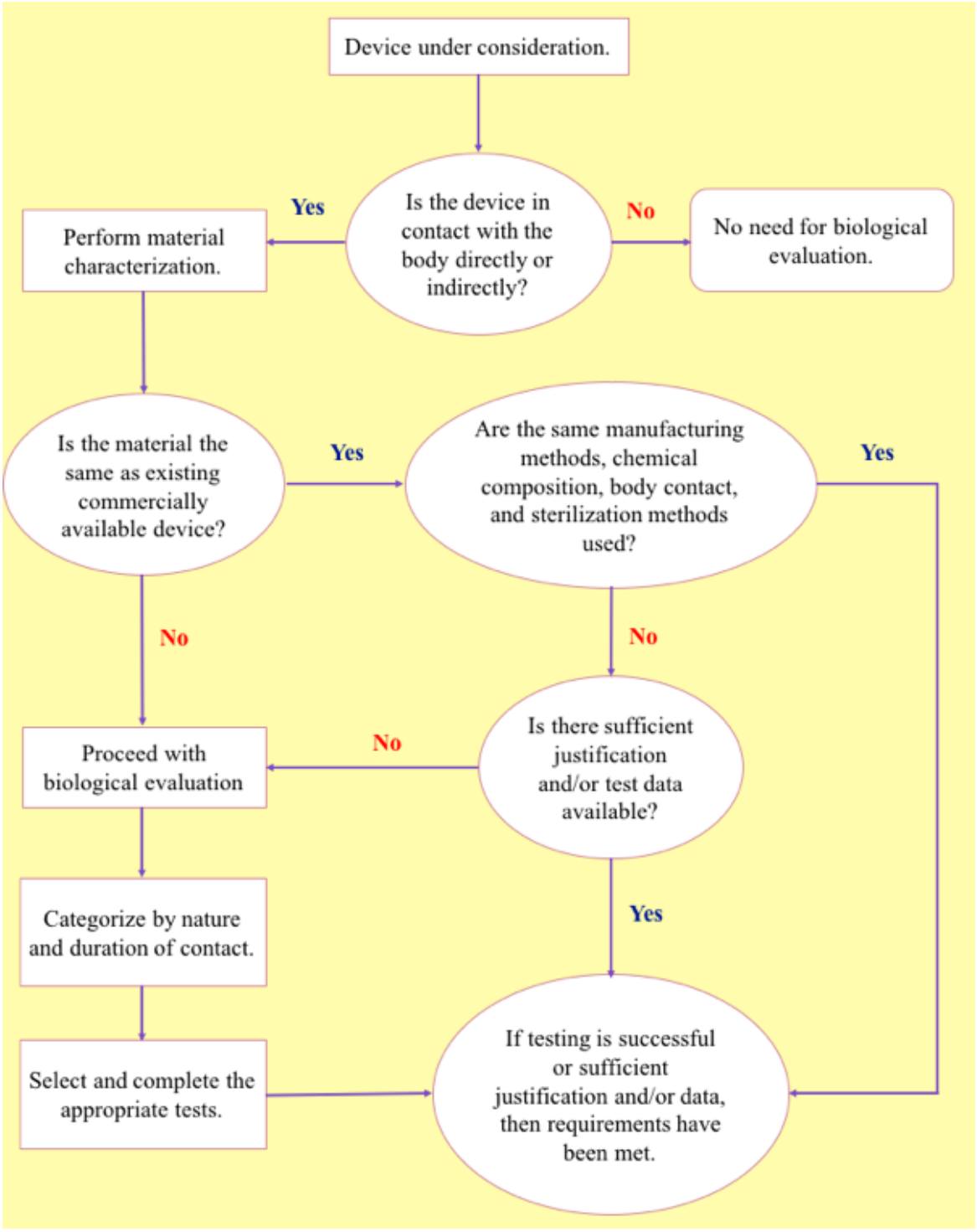

Figure 6 Flowchart guide for biological evaluation of medical devices [44].

As per the flowchart, if there is sufficient justification and/or test data available, then the requirements have been met and biological evaluation or biocompatibility testing is not necessary to be done. Also mentioned by Anderson [45], if a material and its components are well known including the procedures of manufacturing, processing and sterilization have been characterized, testing may not be necessary.

1.3.2 Common testing methods for biological assessment of biomaterials

Biocompatibility testing of biomaterials that are intended for medical devices use are referred to the American Society of Testing Materials (ASTM) Medical Devices Standards and the International Organization for Standardization (ISO) of medical devices testing (Table 5 and 6). They provide detailed protocols for widely accepted testing procedures [43, 45, 46].

As stated in ISO 10993-1:2009, a material component or a medical device should be done within a risk management process framework, in order to reduce unnecessary testing, including animal test, all available relevant information should be considered. As found in FDA regulations, this following information should be included in a risk assessment evaluation: 1) Literature and other publicly available information, 2) Clinical experience, 3) Animal study experience, 4) Medical device standards, and 5) Devices previously reviewed by FDA. If existing data regarding those 5 points are available, then the biological testing is unnecessary.

There are two common biocompatibility testing, the *in vitro* and *in vivo* evaluation. *In vitro* test means literally as *in glass* provides data on biological interaction that is rapid and inexpensive. However, this test should always be compared to *in vivo* complexity of body system and the parameters measured somehow found to be sufficient to represent the body response. *In vitro* test minimizes the use of animal testing and is usually done for a device to get a clinical application approval. *In vitro* test, in most cases, are usually conducted to provide favorable insights whether a material or device need to be further tested with an expensive *in vivo* evaluation test [45].

The experimental design for *in vivo* evaluation testing should consider the great range of animal anatomy, physiology and biochemistry. Animal model selection should be adjusted as best as possible with the aim of the test, therefore the data provided are appropriate to predict the material or device performance in human body. This test should be designed with minimum number of animals used, while still providing the maximum relevant information. To conduct this test, usually an approval from Ethics Committee is needed and by applying the rules of 3R (Reduce, Replacement, Refinement) and the Five Freedoms in animal welfare [45].

Table 5 ASTM standard procedures for different purpose test [47].

No	Test	ASTM standard	
1	Cell-culture cytotoxicity assays	F813	Standard practice for direct contact cell culture evaluation of materials for medical devices
		F895	Standard test method for agar diffusion cell culture screening for cytotoxicity
		F1027	Standard practice for assessment of tissue and cell compatibility of orofacial prosthetic materials and devices
2	Sensitization	F720	Standard practice for testing guinea pigs for contact allergens: guinea pig maximization test
		F2147	Standard practice for guinea pig: split adjuvant and closed patch testing for contact allergens
		F2148	Standard practice for evaluation of delayed contact hypersensitivity using the murine local lymph node assay (LNNA)
3	Skin irritation	F719	Standard practice for testing biomaterials in rabbits for primary skin irritation
4	Mucous membrane irritation	F748	Standard practice for selecting generic biological test methods for materials and devices
5	Intracutaneous injection	F749	Standard practice for evaluating material extracts by intracutaneous injection in rabbit
6	Systemic injection acute toxicity	F750	Standard practice for evaluating material extracts by systemic injection in the mouse
7	Blood compatibility:		

	Thrombogenicity	F2382	Standard test method for assessment of intavascular medical device materials on partial thromboplastin time (PTT)
	Hemolysis	F756	Standard practice for assessment of hemolytic properties of materials
	Complement activation	F1984	Standard practice for testing for whole complement activation in serum by solid materials
		F2065	Standard practice for testing for alternative pathway complement activation in serum by solid materials
8	Pyrogenicity	F748	Standard practice for selecting generic biological test methods for materials and devices
9	Carcinogenesis	F748	Standard practice for selecting generic biological test methods for materials and devices
10	Implantation tests:		
	Short term subcutaneous	F1408	Standard practice for subcutaneous screening test for implant materials
	Short term intramuscular	F763	Standard practice for short-term screening of implant materials
	Implantation testing for biological response to particles	F1904	Standard practice for testing the biological responses to particles *in vivo*
	Long term implant test	F981	Standard practice for assessment of compatibility of biomaterials for surgical implants with respect to effect of materials on muscle and insertion into bone
11	Immunogenicity	F1905	Standard practice for selecting tests for determining the propensity of materials to cause immunotoxicity
		F1906	Standard practice for evaluation of immune response in biocompatibility testing using ELISA tests, lymphocyte, proliferation, and cell migration
12	Mutagenicity	F748	Standard practice for selecting generic biological test methods for materials and devices

Table 6 Biological evaluation of medical devices on ISO standards.

Test	ISO standards
Part 1: Evaluation and testing	10993-1:2003
Part 2: Animal welfare requirements	10993-2:2006
Part 3: Tests for genotoxicity, carcinogenicity and reproductive toxicity	10993-3:2003
Part 4: Selection of tests for interactions with blood	10993-4:2002
Part 5: Tests for *in vitro* cytotoxicity	10993-5:1999
Part 6: Tests for local effects after implantation	10993-6:2007
Part 10: Tests for irritation and delayed-type hypersensitivity	10993-10:2002
Part 11: Tests for systemic toxicity	10993-11:2006

1.3.2.1 *In vitro* test

Cell culture systems is the most common type of test used to evaluate the toxicity of a material or compound toward cells or known as cytotoxicity. Cells are also tested for their adhesion, activation or death to measure biological compatibility. This test is widely used in evaluating new biomaterials compatibility and is required in biocompatibility assessment programs for products such as biomaterials, medical devices and prostheses. In general, there are three types of cell culture assays used for biocompatibility assessment, that is test on extract, direct, and indirect contact test (Table 7). Test on extract or extract dilution type of assay requires a biomaterial extracts, which compounds usually dissolved in a solution such as culture medium, the most common solution used. This test usually conducted at various dilutions, to investigate cytotoxicity and cellular interaction. Small molecular weight extractable are of concern regarding biocompatibility, it has a potential cytotoxicity and the test able to identify the cytotoxic possibility of material within a biomaterial [43, 45].

Direct contact evaluation commonly used to study the biocompatibility of new biomaterials, where an investigator can use the suitable cell type with the biomaterials' intended clinical use. For example, osteoblasts or osteoblast cell lines are used for orthopedic application biomaterials evaluation, investigating the biocompatibility and cell function while in contact with the material. Cardiovascular devices, vascular grafts or prosthetic heart valves use human or animal endothelial cells. Hemocompatibility study use blood cells, either red or white, as well as inflammation or foreign body response studies which usually use primary cells from blood [45].

In vitro cytotoxicity is an initial biological compatibility, which is considered as a screening test for a wide variety of medical devices and biomaterials. A series of test, which are more application-specific, are conducted following the determination of cytotoxicity profile of a biomaterial. The tests are performed to evaluate the biocompatibility as the end-use applications. As screening step, biomaterials that are determined as safe or non-toxic in cytotoxicity test will not be toxic in *in vivo* test. On the contrary, those identified as toxic *in vitro* need to be assessed more for clinical acceptability, as mentioned above in risk

assessment evaluation. Cytotoxicity test is not without problems. The most common problems found are first, the short test duration, which are usually conducted in hours to a few days, and second, the choice of cell type used for the test. The short duration of the test is sufficient to determine important parameters, such as cell proliferation or cell death (necrosis, apoptosis, or cell detachment). The use of cell lines either from human or animals, commonly without understanding of the positive or negative attributes of phenotype expression when compared to the primary cell intended for biological response and cytotoxicity evaluation. Critics are often addressed to *in vitro* test because of the lack in significant metabolic activity from cells. The assays are only able to evaluate innate toxicity of a chemical, not the metabolic products which may have greater or lesser potential toxicity [45].

Table 7 *In vitro* cytotoxicity tests for biomaterial, adapted from [45].

In vitro cytotoxicity test		Principal
Test on extracts	Elusion test	Toxicity is measured by exposing cells on monolayer culture with material extracts in culture medium at a certain time point [48].
	Neutral red uptake test	Viable cells will take up neutral red dye by active transport and incorporate it with lysosomes, while non-viable cells will not take up the dye [49].
	Colony formation test	Cell survival assay based on the ability of a single cell to grow into a colony (defined to consist of at least 50 cells). The assay tests every cell in the population for its ability to undergo "unlimited" division. This test uses to determine cell reproductive death after treatment material or its extracts [50].
	MTT and related test	MTT is a colorimetric assay to assess cell metabolic activity. Viable cells with active metabolism convert MTT into a purple colored formazan product with an absorbance maximum near 570 nm. Whereas died cells will not convert MTT [51].
Direct contact test		Materials are directly exposed to cell culture allowing a physical contact between cells and materials

1.3.2.2 *In vivo* test

In vivo test is done to assess the biocompatibility of biomaterials or medical devices and to determine its performance in the body environment, simulates the end-use applications. The

test is useful to evaluate the potential harm or adverse reactions to the patient. The standardized procedures, protocols and guidelines to conduct this *in vivo* assessment test for the medical device biocompatibility are provided by ASTM, ISO, and USP as the regulatory bodies together with FDA as the government agency. To perform an appropriate *in vivo* test, firstly the biomaterials components are categorized by the site of implantation or tissue-device contact and the duration of the contact. The categorization is shown in the Table 8, which is derived from standards, protocols and guidelines that have been used before for medical device safety evaluation purposes. According to the table, some devices can be categorized in more than one category. In this case, appropriate tests should be done for each category. Table 8 presents tests requirements according to the specific types and contact duration of biomaterials [45].

Table 8 Medical device categorization by tissue contact and contact duration. Adapted from [45].

Medical devices	Tissue contact	Contact duration
Surface devices	Skin Mucosal membranes Breached or compromised surfaces	Limited, ≤24 hours Prolonged, >24 hours and <30 days Permanent, >30 days
External communicating devices	Blood path, indirect Tissue/bone/dentin communicating Circulating blood	
Implant devices	Tissue/bone Blood	

Preliminary *in vivo* tests are commonly performed to gain some insight of the general tissue responses and compatibility, to determine the unknown chemical which can trigger adverse reactions, if any. This early assessment usually conducted for newly developed biomaterials. The information is useful for further development and research, such as the appropriate design criteria and also for manufacturing the final product. This purpose serves as the first perspective of *in vivo* biocompatibility assessment. The second one focuses on the biocompatibility of final product. The devices and its component are in the condition mimicking the implantation in patients. In this condition, devices implanted in selected animal models to assess their function and compatibility. Appropriate tests but unnecessarily all that recommended, may be performed on biomaterial component devices

that have been prepared under processes (manufacturing, sterilizing and other) utilized in the final product development [9, 45].

In vivo tests are done to assess local and systemic responses of materials and devices implantation (Table 5: 2-12). The information provided from this test are irritation and sensitization reactions, intracutaneous reactivity, blood compatibility/hemocompatibility, acute and chronic as well as local and systemic inflammation, genotoxicity, carcinogenicity, reproductive and developmental toxicity, biodegradation, and immune responses [52, 53].

Chapter 2 Description of the Project

2.1 Research questions

Based on the literature review in the previous chapter, a general question arises: Do biodegradable metals have potential for biodegradable ureteral stent applications? Because this thesis focuses on *in vitro* investigation, it can be derived into two specific questions, 1) What are the effects of their degradation on urothelial cells health and function? 2) How the tissue-engineered ureter behaves in presence of the degrading metals?

2.2 Objectives

The general objective of the project is to define the cytocompatibility of biodegradable metals under a simulated ureteral environment. It is then formulated into two specific objectives, i.e. 1) to determine the degradation behavior of BM in simulated urological condition; and 2) to assess their cytocompatibility toward urothelial cells with direct and indirect toxicity

2.3 Hypothesis

Owing their high inherent strength, controlled biodegradability and good cytocompatibility, biodegradable metals such as iron, magnesium, zinc, and their alloys must have a potential for ureteral stent applications.

Chapter 3 Materials and Experimental Methods

3.1 Materials and extract preparation

Biodegradable metals used in this project are pure iron, pure magnesium, pure zinc, and the alloys of Mg-2Zn-1Mn (ZM21), Zn-1Mg and Zn-0.5Al in the form of solid rods. All metals were obtained through collaboration with Prof. Maurizio Vedani, Politecnico di Milano, Milan, Italy.

Two zinc alloys (Zn-1Mg, and Zn-0.5Al) and one magnesium alloy (Mg-2Zn-1Mn) were prepared via casting and extrusion as detailed in Mostaed, et al. [54]. Briefly, high purity magnesium (99.95%), zinc (99.99%), and aluminium (99.99%) were melted at 500°C inside an electronic resistance furnace to produce cast cylindrical billets which then homogenized at 350°C and extruded. The alloys were made into powders by mechanical filing using steel file, whilst small disks were cut for use in potentiodynamic polarization (PDP) test and direct 3D cytotoxicity assay. The specimens were cut into disk using a slow speed diamond rotating blade (Isomet 1000 Precision Saw, Buehler, Uzwil, Switzerland). The specimens for PDP were cut at a thickness of 4 mm and were then polished using SiC paper from #600, to #800, and to #1200 (Carbimet 2 Abrasive Paper, Buehler, Uzwil, Switzerland). The weight of metal disks for direct 3D test were 355±0.01 mg (ZM21), 801±0.02 mg (Zn-1Mg), and 437±0.00 mg (SS316L) with surface area ~200 mm^2. Specimens of pure iron, pure magnesium and pure zinc were used as control. Furthermore, the size of the powders and the surface of metal disks were measured by using SEM (JEOL 7500-F, JEOL Ltd., Tokyo, Japan).

The artificial urine (aU) was preferred in this study to natural urine to have more reproducible results. The aU solution was prepared from analytical grade chemicals (Sigma-Aldrich, St. Louis, MO, USA) with composition presented below (Table 9). The aU was kept at 37 ± 1°C using a water heater and a jacketed beaker, stirred with a magnetic stirrer at 80 rpm. The pH of the aU was adjusted to 6.0 by adding 1 N NH_4OH and monitored with a pH meter (Accument pH meter 25, Fisher Scientific, Portsmouth NH, USA).

Table 9 Artificial urine composition [55].

Chemical	NaCl	NaH_2PO_4	$Na_3C_6H_5O_7$	$MgSO_4$	Na_2SO_4	KCl	$CaCl_2$	$Na_2C_2O_4$
Mass (g)	6.17	4.59	0.944	0.463	2.408	4.75	0.638	0.043

Metal disks were sterilized under UV for at least 1 hour. Furthermore, metals were immersed in 30 ml artificial urine and incubated in 37°C with 5% CO_2. After 1, 6, 12, and 24h, 10 ml of solutions was collected from each metal and another 10 ml of fresh aU was added to replace the lost volume. The collected solutions were filtered using 0.22 µm Durapore® PVDF membrane filter (Millex® GV, Merck Millipore, Ltd., Darmstadt, Germany) to eliminate precipitate and then stored at 4°C prior to use. These solutions were used for viability screening test.

On the other hand, metal powders were sterilized under UV for at least 1 hour, mixed with urothelial cell (UC) basal media: DMEM and Ham F12 3:1 supplemented with 10% fetal bovine serum, 5 µg/ml insulin (Sigma), 10 µg/ml epidermal growth factor (Austral Biologicals, San Ramon, CA), 10^{-10} M cholera toxin (Sigma), 100 U/ml penicillin and 0.4 µg/ml hydrocortisone (Calbiochem, San Diego, CA), and incubated in 8% CO2 at 37°C for 72 hours. The mixing ratio of each metal was 15 mg of Zn, 5 mg of Mg, 36 mg of ZM21, 15 mg of Zn-1Mg, and 12 mg of Zn-0.5Al for each ml of media to prepare the stock solutions.

After the incubation, the solution was filtered using 0.22 µm Durapore® to remove the undisolved metal powder. The stock solutions were then stored at 4°C prior to use. To determine the IC_{50} of the alloy and pure metals, each metal has six different concentrations from each other (Table 10). The six different concentrations were prepared by diluting serially the stock solutions (1st concentration) with UC basal media until the lowest concentrations were reached (6th). UC basal media was used for control. After the IC_{50} value of each metal were determined, metal extracts were then prepared in IC_{50} concentration for cell treatment, also for pH and ion measurement.

Table 10 Metal concentrations prepared for IC_{50} value estimation.

Metals	Concentration					
	1st	**2nd**	**3rd**	**4th**	**5th**	**6th**
Mg	5	3.5	2	1.5	1	0.5
Zn	15	10	8	6	4	2
ZM21	30	28	24	16	10	4
Zn-1Mg	15	14	12	8	6	2
Zn-0.5Al	10	9.5	8	6	4	2

3.2 Cell culture and flat 3D tissue-engineered ureteral model

Normal human urothelial cells (NHUCs) from a human pelvic renal biopsy with local ethic committee approval as described by Magnan et al. [56]. NHUCs were cultured with irradiated mouse 3T3 in UC basal media and incubated in 8% CO_2 at 37°C. Detailed explanation will be presented in sections below. Each test to assess cell health was conducted with 5 replicates.

The procedure for producing tissue models explained schematically in Figure 7 and was adapted from bladder model as described by Chabaud et al. [57]. In brief, normal primary human dermal fibroblasts were seeded at 4 x10^4 cells/cm^2 in 6 well-plates which has been previously filled by a ring of filter paper used as anchorage for the stroma. The cells were cultured in DMEM supplemented with 10% newborn calf serum (NBCS), 100 U/ml penicillin, 25 μg/ml gentamycin (fibroblast medium) and fresh 50 μg/ml ascorbic acid (Sigma), incubated in 8% CO_2 at 37°C. The media was changed every 2 days and stroma sheets were formed after 20 days of culture. Further step was to make ureteral tissue model/ureteral equivalent (UE). NHUCs were seeded at 2 x10^4 cells/cm^2 on each stroma in UC basal media, supplemented with fresh 50 μg/ml ascorbic acid and incubated in 8% CO_2 at 37°C for 7 days under submerged conditions. The UEs were then moved on air/liquid supports in petri dishes to provide elevation at the air-liquid interface for 14 days. The interface provided aims to promote the differentiation of the monolayer of urothelial cells into mature urothelium.

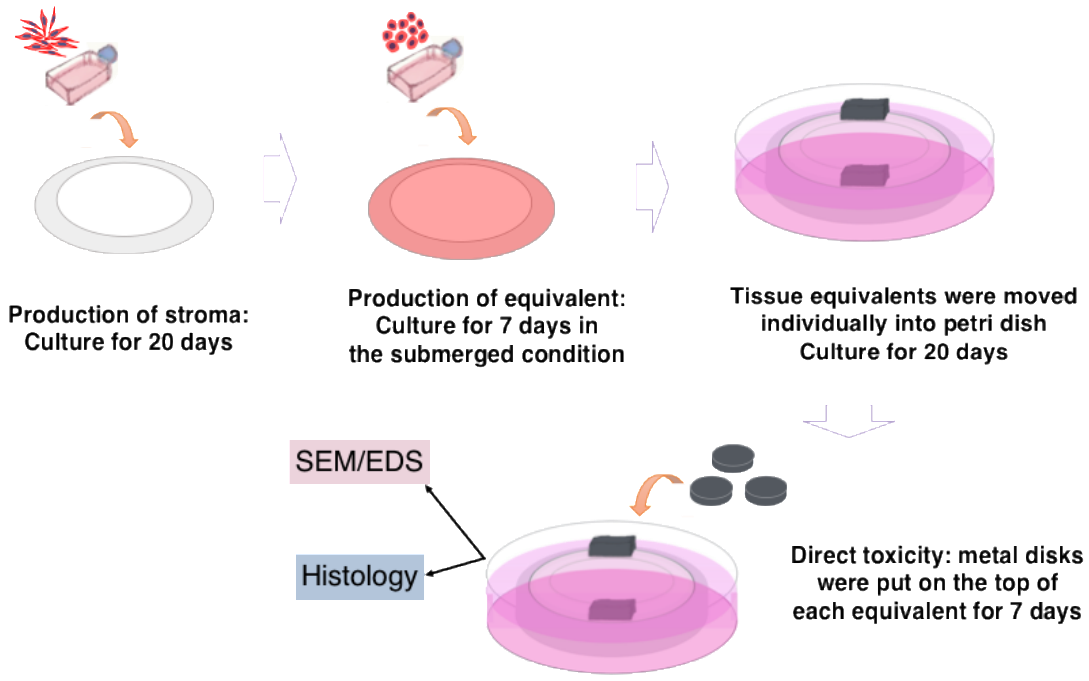

Figure 7 Schematic explanation of the flat 3D tissue engineered/UE production and direct toxicity test.

3.3 Cell viability test

Screening and inhibition concentration 50 (IC_{50}) estimation

Cell viability test for screening the pure metals and to estimate the IC_{50} of pure Mg, pure Zn, Mg-Zn and Zn-1Mg, an indirect viability test was conducted using Water Soluble Tetrazolium (WST) mitochondrial assay with WST-1 reagent (Takara, ClonTech, Germany). 5.0 $x10^4$ NHUC were seeded in 96-well plate and left overnight to let the cells attach. For screening test, the solutions collected from different time of incubation were used to treat the cells. For IC_{50} estimation, the metal extracts at 6 different concentrations, ranging around the value determined during preliminary tests, were poured into the wells replacing the UC basal media. The metal extracts were removed after 24 h of incubation, and the cells were washed with sterile phosphate buffer saline (PBS) twice. 10% WST-1 reagent diluted in UC basal media were added to each well and incubated for 30 minutes. The optical density was measured at 440 nm using a microplate reader (Varioskan® Flash,

Thermo Fisher Scientific, US). Percentage of cell viability were calculated using the following formula [58]:

Equation 1

Percentage of cell viability = (OD sample-OD blank)/ (OD control-OD blank) x100%

3.4 Cytoskeletal observation

Guinea pig antibody raised against human keratin 8/18 (ARP, Belmont, MA) and Hoechst 33342 (Thermo Scientific) dye were used as the primary antibodies to visualize keratin intermediate filaments and nuclei, respectively. 2 x 10^5 NHUCs were seeded in coverslip containing 24-well plate and incubated with 0.5 ml of metal extracts for 1 and 3 days at 37°C with 8% CO2. The cells were fixed on chamber slides using cold methanol for 10 minutes at -20°C and then washed thoroughly with PBS. Then, 50 µl of anti-keratin 8/18 antibody diluted 1:50 in PBS-BSA 1% was added and incubated for 45 minutes. After discarding the first antibody, the cells were rinsed using PBS. Then, 50 µl of Alexa-594 coupled with secondary antibody (Sigma) diluted in PBS-BSA 1% was added, incubated for 30 minutes in the dark, and washed with PBS three times for 2 minutes each, and washed with distilled water twice. 50 µl Hoechst (1:100) staining to visualize the nucleus diluted in PBS-BSA 1% was then added for 10 minutes of incubation in the dark and washed with distilled water three times. A drop of mounting medium, PBS-glycerol-gelatin (pH 7.6), was put on the slide, and the invert coverslip on the top of the drop. The slides with coverslip were put in 4°C overnight to make sure the mounting medium was solid. The slides were then viewed under Fluorescence Microscope with ApoTome attachment (Zeiss-Axio Imager Z1, Toronto, CA).

3.5 Cell function evaluation on 3D UE

Direct toxicity test was conducted to assess the urothelial cell function. Metal disks were sterilized with UV light exposure for 15 minutes on each side, then dipped in ethanol 3 x 5s and washed with PBS, under the hood. Metal disks were put on the UEs and incubated for 7 days. The direct toxicity test was done with 4 replicates, furthermore, 5 replicates were used for each histological observation.

After each incubation time, UEs in all groups were sacrificed by cutting UE into two halves. First half was fixed with Histochoice tissue fixative (Amresco, Solon, OH) and then embedded in paraffin. The procedure was as previously described by Imbeault et al. [59]. Histological sections were made by cutting paraffinized tissue into 5 μm in size and stained using Masson Trichrome protocol. Second half was embedded in frozen tissue medium (OCT compound; Tissue-Tek, Bayer, Etobicoke, Canada) for further evaluation by immunofluorescence. Uroplakin staining was done on paraffinized tissue slices, as described by Cattan et al. [60], thus in this case, tissue slices needed to be deparaffinized before the immunostaining. Briefly, the glass slides containing tissue slices were deparaffinized by washing with xylene 3x for 5 min each. Slides were then washed in serial decreasing concentration ethanol solutions, 100%, 90%, 80%, 70%, and 50%, 5 min each and rehydrated under running water. Antigen retrieval was done by soaking slides into citric buffer with 0.05% Tween 20 pH 6.0 and then boiled in microwave for 3x 10 min. Furthermore, the slides were cooled down at room temperature for 20 min, followed by washing under running water. Slides were then ready to be immunostained. The slides from both paraffinized and OCT were fixed in cold 100% methanol, blocked with PBS-BSA 1%, and incubated with primary antibodies, as described in the procedure of cytoskeletal observation above. Primary antibodies used were raised against laminin (Sigma), uroplakin 2 (Santa Cruz Biotechnology), ZO-1 (Invitrogen), and Ki-67 (Abcam). Secondary antibodies were coupled with Alexa-488 and -594 fluorochromes. The slides were then viewed under Fluorescence Microscope with ApoTome attachment (Zeiss-Axio Imager Z1, Toronto, CA) [61].

3.6 Scanning electron microscopy

Metal disk remnants were preserved in 2.5% glutaraldehyde overnight in 4^{o}C and processed for further observation under electron microscopy as described by Heckman et al. [62]. After overnight incubation, remnants were washed with PBS 3x5 minutes and then dehydrated by using serial ascending concentrations ethanol solutions from 30%, 50%, 70%, 90% for 5 minutes each, and then 3x5 minutes in 100% ethanol. The remnants were

dried and then gold sputtered. Observation were done by using SEM (JEOL 7500-F, JEOL Ltd., Tokyo, Japan).

3.7 pH and ion measurement

The pH value of metal extracts was measured by a pH meter (Beckman Coulter PHI 350; Beckman Coulter Life Sciences, Missisauga, ON). In brief, the pH meter was calibrated using 3 pH standard solutions (pH 4, 7 and 10) at room temperature. The sample solutions that were previously reheated until 37°C to have the same conditions when the cells are being treated, were poured into a small beaker and measured repeatedly.

The level of ion released of the extraction media was measured by inductive coupled plasma mass spectrometer (ICP/MS) [63-65] for the three metal ions, Zn, Mg, and Al. In brief, the extracts were digested for 3 days before the ion measurement. At day 1, 3 ml of extracts were added into the vial, then a mark was drawn to show the meniscus level of 3 ml. In a fume hood, the crystallizer was filled with paraffin oil prior to vial holder mounting to avoid oil splash. The vial holder was then mounted, and it should not touch the crystallizer bottom surface, and the vial should be half immersed in the oil. The oil was heated until 90°C and 3 ml HNO_3 was added to the vial, then the temperature was raised to 115°C. When the solution inside the vial became 3 ml by observing the mark, another 3 ml HNO_3 was added. After the solution evaporated and 3 ml left inside the vial, the oil bath was lifted and air dried. Then it was placed on a paper towel to absorb the excess oil. The treatment at day 2 started with the addition of 600 µl nanopure water and 900 µl of 30% H_2O_2 into each vial. Then the oil bath bottle was heated at 115°C until the excitement phase appeared. Attention should be paid to make sure that no drop of oil is lost by an excessive excitement. The solutions were allowed to heat until it became approximately 3 ml. The oil bath then was lifted and air dried, and then placed on a paper towel to absorb the excess oil. At day 3, the solutions were transferred into 5 ml volumetric flask, whilst the vial was rinsed with 3 ml nanopure water; the water then was poured into the volumetric flask to complete 5 ml. The solutions were then transferred into centrifuge tubes and ready to be analysed. The solutions were then analyzed with ICP/MS equipment (5110 SVDV, Agilent Technology, Santa Clara, CA, USA).

3.8 Potentiodynamic polarization

The metal specimens were mounted as working electrodes in a waterproof chamber with an exposed area of 0.096 cm^2 (0.35 cm of diameter), and all tests were done in triplicate for statistical analysis. The PDP was performed on all metal specimens using a three-electrode cell configuration. The metallic samples served as the working electrode, a graphite rod as the counter electrode, and a saturated calomel electrode (SCE) (E=+0.241 V saturated) as the reference electrode. The electrodes were connected to a VersaSTAT3 potentiostat and monitored using the VersaStudio software (Ametek Princeton Applied Research, Oak Ridge, TN, USA). The PDP tests were done using a scan rate of 0.6 V/h, from -0.25 to +0.6 V.

3.9 Data analysis

All results were expressed as mean ± standard deviation of each independent experiment. The statistically significant difference between the mean was calculated by ANOVA and post hoc Tukey test for multiple comparisons with the level of significance to be selected at $p<0.05$ using SPSS 25.

Chapter 4 Results and Discussion

4.1 Screening test

The goal of this study was to find which metal(s) could be used for ureteral stent application, to assess their biological compatibility toward urothelial cells, and to establish the protocols of assessment. The study started with a serial of screening tests that were divided into 2 parts. In the first part, three most mentioned and studied biodegradable metals, high purity Fe, Mg, and Zn were used. The tests included the WST mitochondrial assay to assess the cell viability after 3 days treated with metal extracts in artificial urine (aU) solution. The last test for the screening part was potentiodynamic polarization (PDP) to determine the Tafel slopes and corrosion current density [66], therefore their corrosion rate in aU solution can be predicted. PDP was done in another study as a part of Dr. Hermawan's project.

4.1.1 Cell viability

Figure 8 shows the result of cell viability test with WST mitochondrial assay on NHUCs after 24 h of incubation with metal extracts in aU solution. Pure Fe had the lowest viability compared to pure Mg and Zn from the first hour until 24 h of incubation. Pure Mg followed after with an increased cell viability along with the metal incubation time. Meanwhile, pure Zn had the highest cell viability and the trend was constant from 1 h to 24 h of incubation.

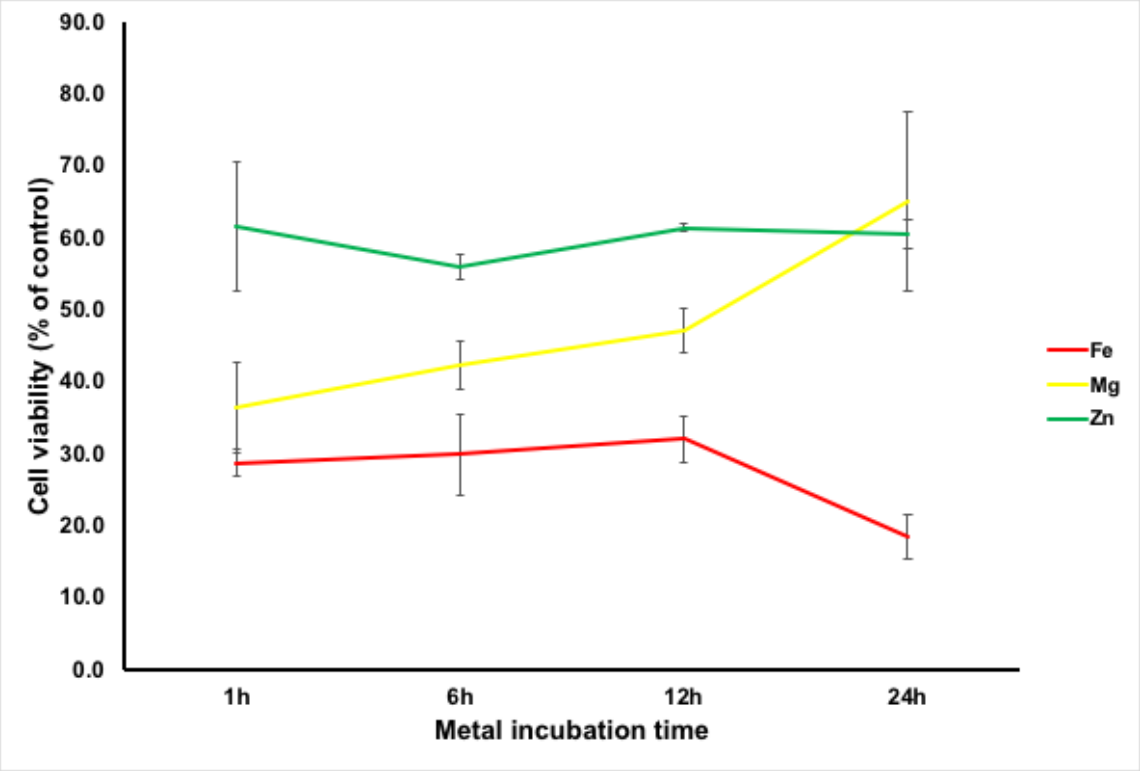

Figure 8 NHUCs viability after cultured with pure Fe, Mg, and Zn extracts in artificial urine solution with different incubation time.

The slow degrading Fe showed the lowest, while Mg showed increasing trend in cell viability. The explanation for this could be because the excessive Fe ions form free radicals and causes oxidative stress. The free radicals react with organic molecules in the cell membrane, start a lipid-peroxidation process and eventually lead to cell death [67]. The increasing trend of Mg might be due to the formation of salts. The salts may include $Mg(OH)_2$, Mg3(PO4)2, MgCO3, Ca(OH)2, Ca3(PO4)2, CaCO3, and related salts as mentioned in a study by Witecka et al. who observed the degradation of Mg-alloys in buffer solutions [68]. The more salt formation, the less Mg^{2+} interact with the cells. The environment is considered unfavorable for the cells when the degradation products such as Mg^{2+} and OH^- reach certain concentration [69]. The constant trend on Zn viability was caused by the constant degradation of Zn^{2+} ions into the artificial urine from the 1st until 12th hours of metal immersion.

4.1.2 Potentiodynamic polarization

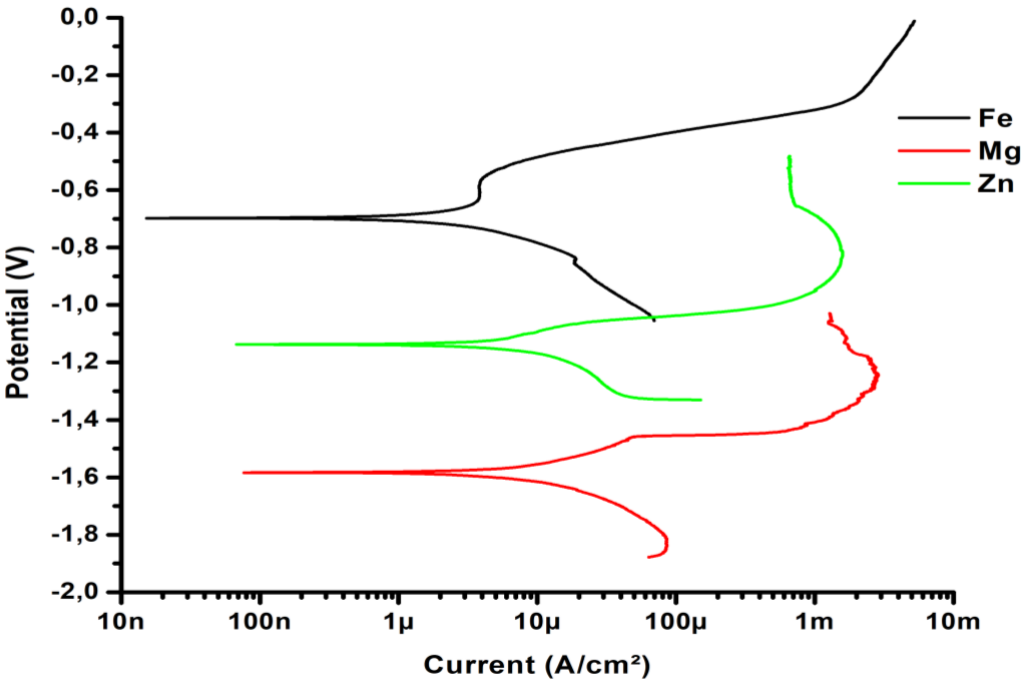

Figure 9 Potentiodynamic polarization (PDP) curves of the pure Fe, Mg, and Zn [70].

Table 11 Corrosion parameters of the pure Fe, Mg, and Zn in artificial urine solution derived from the PDP curve [70].

Sample	i_{corr} (µA/cm²)	Corrosion rate (mm/year)
Fe	6.09 ± 1.02	0.04 ± 0.008
Mg	94 ± 37	2.16 ± 0.84
Zn	58 ± 6	0.87 ± 0.09

The corrosion or degradation rate of the pure metals in artificial urine was confirmed by PDP test. The results are presented in Figure 9 and Table 11, it can be seen that iron has the slowest degradation with 0.04 ± 0.008 mm/year, followed by Zn 0.87 ± 0.09 mm/year and Mg 2.16 ± 0.84 mm/year. The fast degradation of Mg could cause more ions released into the aU solution and the change in pH value. From the first part of this screening test, iron was eliminated because of its slow degradation rate and being the most toxic metal toward urothelial cells compared to pure Mg and Zn.

4.1.3 IC_{50} estimation

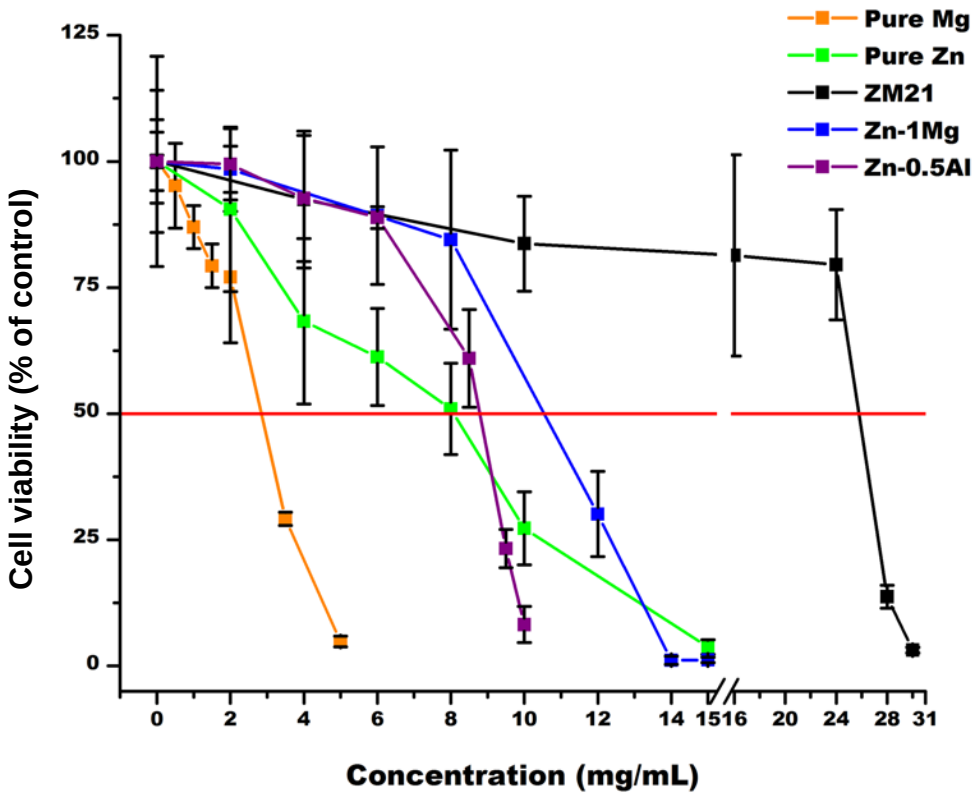

Figure 10 Cell viability with WST mitochondrial assay after 24 h of incubation with metal extracts in culture media. Six different concentrations were used to determine the estimated IC_{50} concentration. Red line marked the 50% of viable cells corresponded with metal extracts concentration to be estimated.

The preliminary viability test used 6 different concentrations for each metal (Figure 10). Based on the results, it is estimated that ZM21 has the highest IC_{50} with concentration measured 25 mg/ml, followed by Zn-1Mg 10 mg/ml, Zn-0.5Al 8.75 mg/ml, pure Zn 8 mg/ml, and pure Mg 3.5 mg/ml, respectively. The estimated IC_{50} concentration values were then used for further assessment.

4.1.4 Physiochemical test: pH and ion release

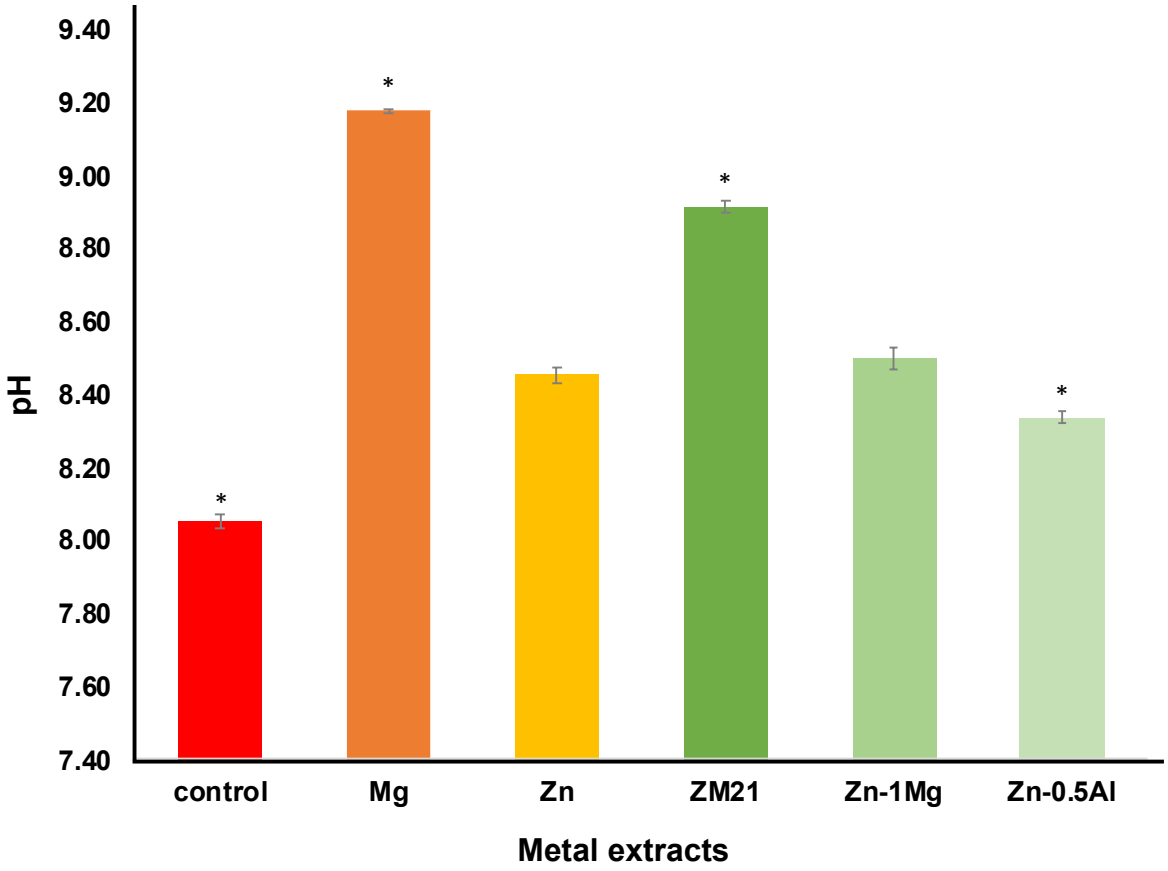

Figure 11 pH value of metal extracts after 72 h of incubation. *p<0.05.

Figure 11 shows pH value of metal extracts after 72 h of incubation. Metal extracts pH are higher than culture medium as control (8.05). The highest is pure Mg extract (9.18), followed by ZM21 (8.91), Zn-1Mg (8.50), pure Zn (8.45) and Zn-0.5Al (8.34).

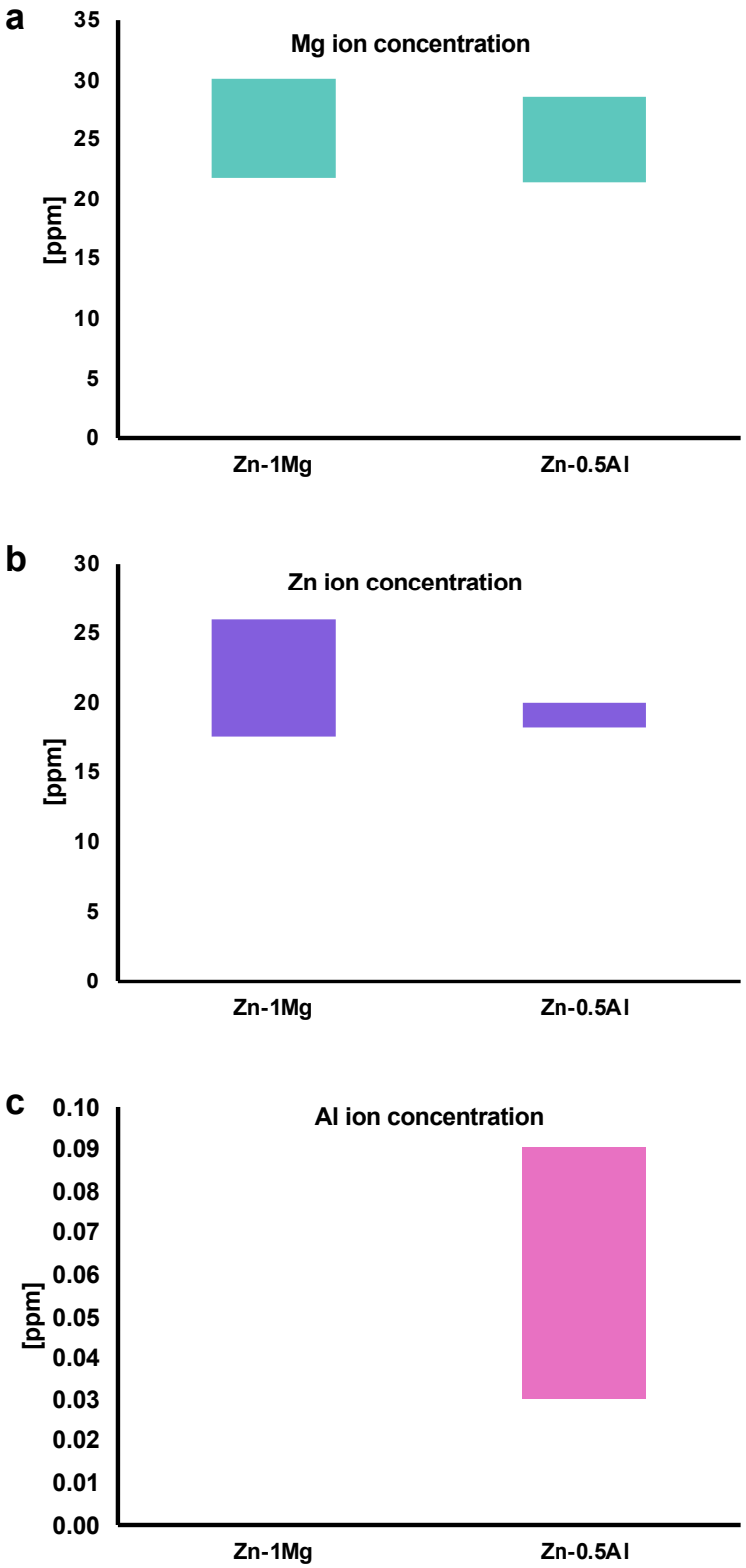

Figure 12 Metal ions concentration in the metal extracts after 72 h of incubation.

The pH of metal extracts is mainly caused by metal ions dissolved in the culture medium and is following this equation [34] :

Equation 2

$M \rightarrow M^{n+} + ne^-$ (1)

$2H_2O + 2e^- \rightarrow H_2 + 2OH^-$ (2)

$2H_2O + O_2 + 4e^- \rightarrow 4OH^-$ (3)

$M^{n+} + nOH^- \rightarrow M(OH)n$ (4)

The product M(OH)n will be transformed into soluble M(Cl)n in culture media and this reaction resulted in the release of OH^- thus alkalinizing the extracts. pH increase influencing cellular functions and compatibility [68]. The faster the degradation, the more OH^- was released, the more rapid alkalinization occurred and the pH value became stable after OH^- reached saturation [32].

It was observed from this experiment that the cell viability is positively influenced by the metal extracts concentration. Pure Mg showed the lowest viability among all metals, with the highest concentration used was 5 mg/ml. ZM21 showed the highest viability with 25 mg/ml estimated IC_{50} concentration. The low viability of pure Mg mainly related to the pH of the extracts. Zn-based groups showed wider range of concentrations, where the highest concentrations used were 10 mg/ml for Zn-0.5Al, and 15 mg/ml for pure Zn and Zn-1Mg. Furthermore, this test was also done to determine the concentration of Zn-alloys to be used in the in-depth tests. The concentrations were estimated from what resulted in 50% of cell viability, hence the concentrations were 10 mg/ml for Zn-1Mg and 8.75 mg/ml for Zn-0.5Al. Similar trend in the relationship between cell viability and ion concentration was also reported by other studies with different type of cells [71-74]. The more metal powder incubated in culture medium resulted in more dissolved metal ions. A study by Tian et al. [69] reported that starting from pH 8.3, urothelial cells were seen unhealthy with round morphology and when pH value reach 8.6 the reduction in urothelial cells' density was significant. The more alkaline was the culture media, the viability of cells were found

reduced. Another study on fibroblasts and keratinocytes found that those cells proliferated, migrated better and were more viable in pH 8-8.7 compared to acidic or more alkaline environment [75]. Recent study by Gu et al. [76] reported that alkaline stress causes severe cytotoxicity in human osteosarcoma cells MG63. Similar result also shown for osteoblasts, the cells had better performance in terms of gene expression and mineralization [77]. A consistently acidic urine pH ≤6.0 is associated with an increased risk of bladder cancer [78]. Based on the result, this test suggests that the Zn-alloys could be chosen as a potential metal for ureteral stent application because they did not alkalinize the culture media toward an adverse level.

Different ion concentration of metal extracts after 72 h of incubation presented by Figure 12. Ion concentration of IC_{50} extracts were measured and the result showed that the highest limit of safe concentration of Zn ions for Zn-1Mg is 25.96 ppm, while Zn-0.5Al is 20.02 ppm (Figure 12a). Mg ions were 30.10 ppm in Zn-1Mg and 28.59 ppm in Zn-0.5Al (Figure 12b). Al ions were only observed in Zn-0.5Al extracts which is 0.09 ppm and none found in Zn-1Mg extracts (Figure 12c). The DMEM-Ham cell media contains Mg ions as per data sheet from the manufacturer. This explains the presence of Mg ions in Zn-0.5Al extracts. Murni et al. [72] reported that 0.49 ppm of Zn ions in the metal extract killed 50% of NHOst cell population. A study by Kubasek et al. [71] found the highest safe concentrations of Zn at 7.85 ppm and 5.23 ppm for U-2 OS and L929 cell lines, respectively. While in this study, the concentration of 25.96 ppm Zn ions killed half of urothelial cell population. The factors that correlated with the different result in the highest safe concentration were also addressed. Different cells that were used in the study by Kubasek showed that a cell line can be more sensitive than another; the authors also compared their result to the other works using different type of cells. Urothelial cells on the other hand, when cultivated in monolayer culture were grown only as a basal cell which is found in the deepest layer of urothelium layers in the native tissue. This causes the sensitivity of urothelial toward the metal extracts to be higher in this study. In addition, urothelial cells used in this study were in passage 2 and harvested from the primary culture. Generally, primary cultures are more sensitive toward toxic substances than cell lines because the cultures are also adapting to the culture conditions [79]. The use of serum

(FBS) in the metal extracts or salt solutions gives protective effect to the cells. It is well known that the use of serum in the culture media in either 5% or 10% induces the growth of the cells and studies reported that the cell viability in cytotoxicity test are higher in those with the presence of serum [16, 71, 80, 81].

4.2 Cell health

Cytoskeletal observation

Cytokeratin (CK) network is presented in Figure 13. It was observed that changes occurred in cell size and morphology in the presence of metal ions. The cells capability to still form colonies even when they are experiencing changes, was noted, but cells in the Zn-1Mg group shrunk and rounded as in apoptotic stage compared to Zn-0.5Al group at day 1. On the contrary, ZM21 group showed scattered cells with rounded up appearance and CK were seen as dots inside of some cells similar to dying cells morphology. The intensity of CK was less in all metal alloy groups compared to controls. Observation at day 3 showed that cells in both alloy groups survived and Zn-0.5Al group had recovered their normal state. While cells in Zn-1Mg group did not recovered fully yet seen from their size and morphology compared to controls, and the intensity of their CK was also less than the other groups. Rounded morphology found in ZM21 and Zn-1Mg group at day 1 could also result from the alkaline pH (8.91 and 8.50) of the culture media. CK were less intense in ZM21 and Zn-1Mg groups compare to controls and Zn-0.5Al group, metal ions binding causing this effect on CK. It would have been interesting to do a time-lapse microscopy experiment to confirm the apoptosis event.

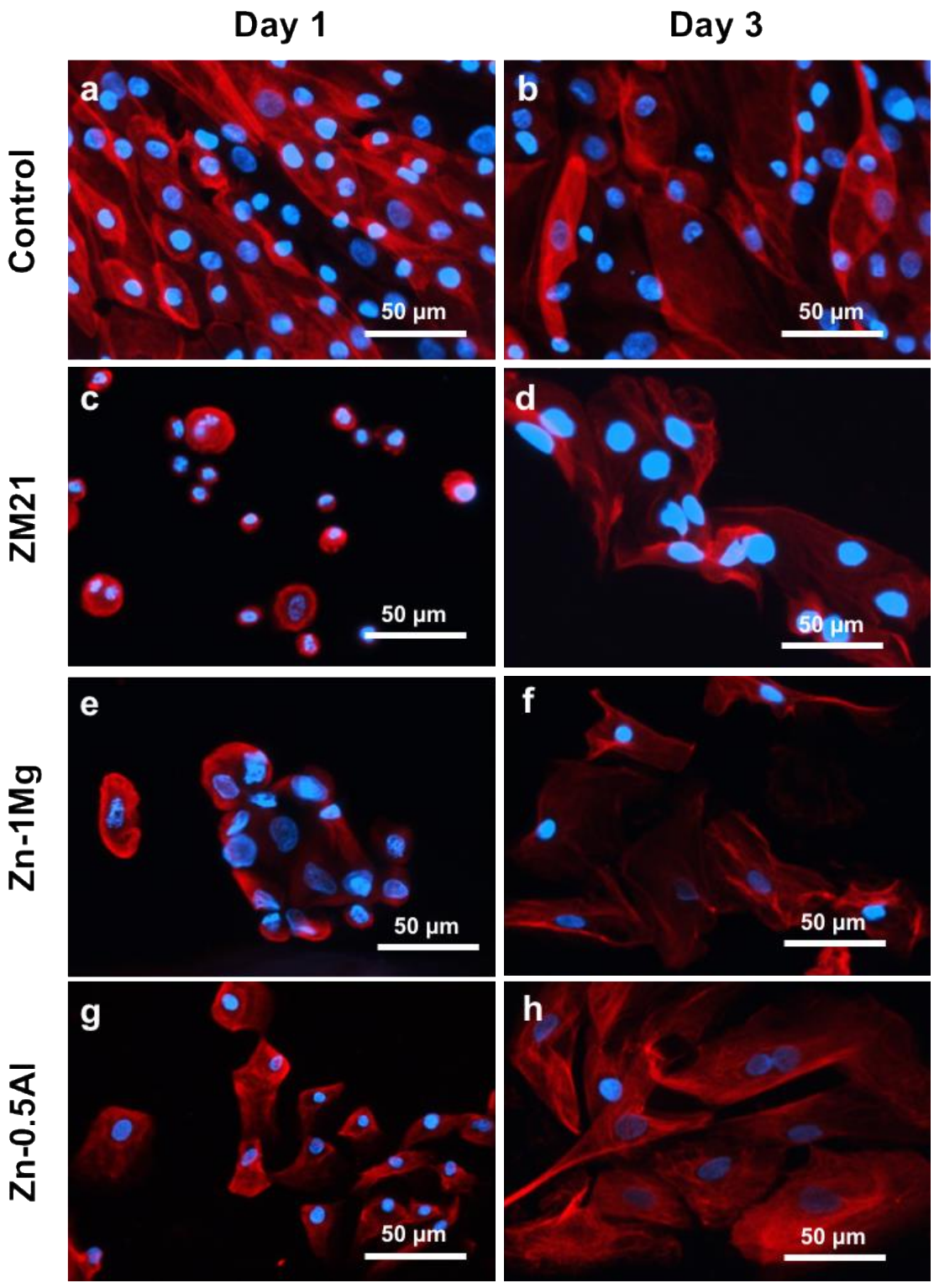

Figure 13 Images of cytoskeletal observation at day 1 and 3 in controls, ZM21, Zn-1Mg, and Zn-0.5Al groups. Note: anti-cytokeratin 8/18 (red) staining was used to examine the changes of keratins, and Hoecsht (blue) was used to stain nucleus of the NHUCs. Bar=50 μm.

Cytoskeletal changes in the presence of Zn ions was reported also by Murni et al. It was observed that the cells were undergoing changes in size, contours and skeletal intensity, which correspond to apoptosis and inhibition of cell proliferation. The adaptation of epithelium to changing conditions usually is accompanied by transition in the cytoskeleton of epithelial cells. Cytokeratin, as a major structural protein in epithelial cells, plays role in mechanical and non-mechanical functions, including protection from cell stress and apoptosis, epithelial polarity, helps in cell-cell adhesion, and also attachment of the epithelial cells with the underlining connective tissue. Besides this structural function, CK also plays a role in dynamic processes such as mitosis, mobility, and differentiation [82, 83]. Cytokeratins 8/18 pair are obligate partners and establish the primary cytokeratin pair in many epithelia including urothelium [84]. CK role in apoptosis has been reported by many studies. The apoptosis process with chromatin condensation as its hallmark is first preceded by the breakdown of CK8/18. The breakdown results in the collapse of cytoplasmic and nuclear cytoskeleton [82].

4.3 Cell function evaluation

As mentioned by Tian et al. [69], cytotoxicity test should closely represent *in vivo* conditions to provide meaningful information. In their study, direct toxicity was done to evaluate possibility of urothelial cells to attach to magnesium-based alloys using three different method in monolayer culture. In our study, direct toxicity was done by putting metal disks on the top of the urothelium of engineered ureteral tissue in flat 3D models, adapted from our established engineered bladder and urethral tissue models using self-assembly method [59, 61]. Since urothelial is a highly-specialized epithelium, the use of flat 3D culture to have similar structure as in native tissue in combination with direct toxicity, is considered as a closest yet simple method to *in vivo* conditions. To our knowledge, this is the first tissue-engineered used to assess metal toxicity. The direct cytotoxicity was done to assess the cell function in the presence of metal disk and its degradation products. This test was also done to observe the effect of compression from the weight of the disk on the engineered ureteral tissue. The disk compression itself simulated the inflated stent in the ureter which compresses the tissue. Ureteral tissue consists of layers

of urothelium which act as a permeability barrier protecting the blood from toxic compounds in the urine.

4.3.1 Macroscopic observation

Table 12 Macroscopically observed changes of UEs after 1 week of observation.

Parameters	Control	ZM21	Zn-1Mg
Tissue appearance	No change	Thick white structure surrounding the peri-metal site	No change
Medium culture (phenol red as pH indicator)	Yellow after 2 days of culture (acidic)	No color change (alkaline)	Yellow after 2 days of culture (acidic)
Metal corrosion product	Not found	Bubbles surrounding the metal	Not found

Table 12 presents the changes observed macroscopically during the incubation of UE with metal disks. ZM21 group has significant changes compared to control and Zn-1Mg group, marked with changes in all three parameters. The macroscopic changes are presented in Figure 14. Thick white structure of ZM21 group surrounding the peri-metal disk site marked in area 3, whilst bubbles were obviously present surrounding the metal. Different shapes of each metal specimens that is shown in Figure 14 were caused by the limited alloy samples and equipment to process them into the same shape. Therefore, those samples have roughly the same surface area of ~200 mm^2. In further study, the metal specimens could have similar form to minimize the differences that may affect the result.

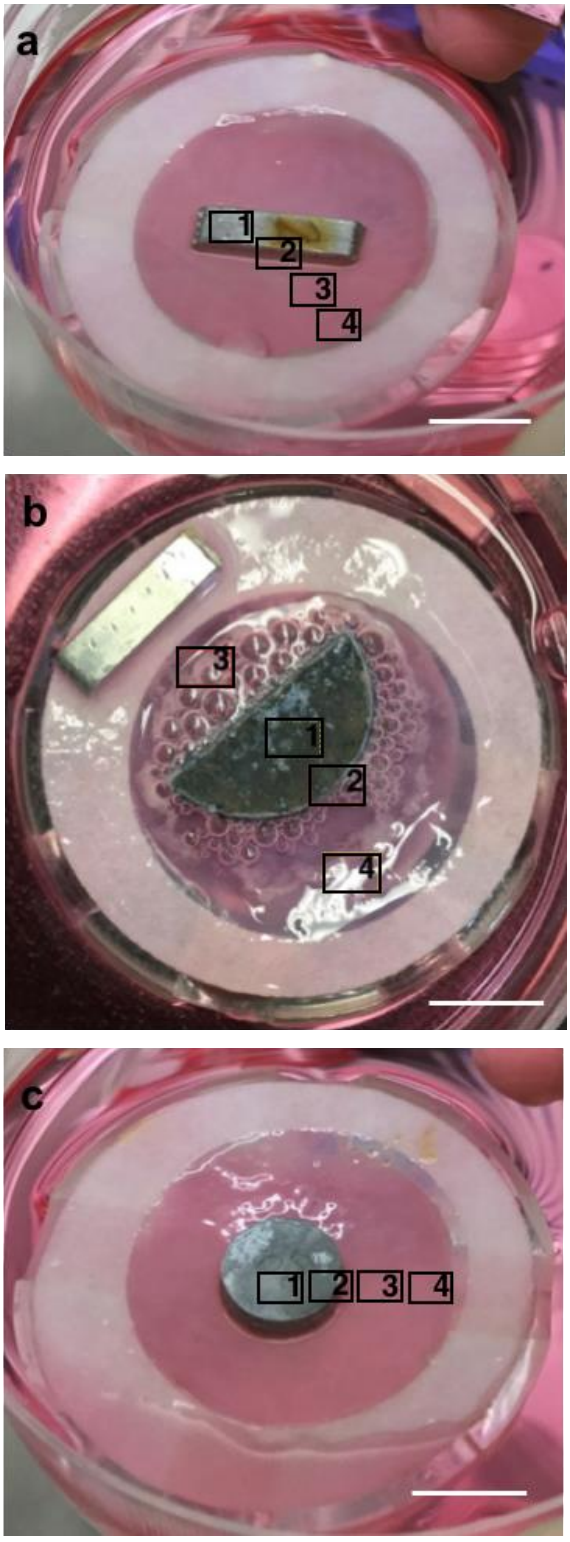

Figure 14 Representative UE with a. control/stainless steel, b. ZM21, and c. Zn-1Mg disks after 1 week of incubation in fresh medium. Histological sections divided into 4 areas based on the distance with metal disk. Area 1, under/in contact with metal disk; area 2, peri-metal site; area 3, nearest area to peri-metal site; and area 4, farthest to peri-metal site. Bar=1cm.

4.3.2 Histology: Masson Trichrome

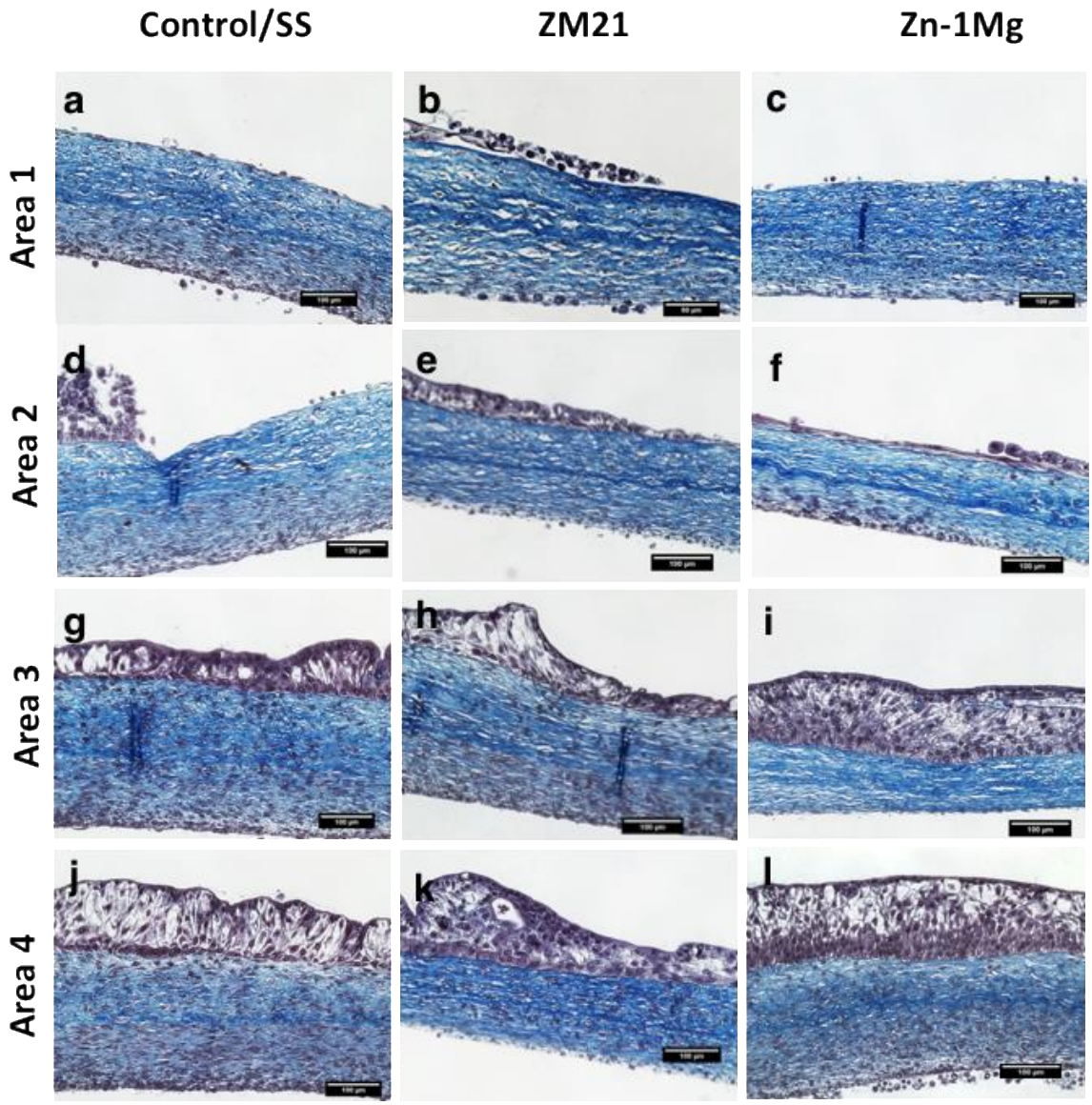

Figure 15 Histological analysis of UEs with different metal disks stained with Masson Trichrome. Urothelial cells stained as purple and stroma/collagen stained as blue. Tissue sections are divided into 4 areas: 1) under/in contact with metal disks, 2) peri-metal site, 3) nearest area to peri-metal site, and 4) farthest area to peri-metal site. Bar=100 μm.

Histological sections stained by Masson Trichrome provides information about the morphology of urothelium in the presence of metal disks and their degradation products. The tissue-engineered ureter used in this study consisted of layers of urothelium and stroma

or connective tissue beneath it to closely mimic a native ureter tissue. The ability of urothelial cells to migrate, proliferate and differentiate to form urothelium is important to maintain the urothelial integrity and to keep the permeability barrier function [85]. Figure 15 shows histological analysis in 4 different areas based on the distance with metal disks, while Figure 14 shows the division of the area. Area 1 in direct contact with or under metal disks was seen with minimum urothelial cells present in ZM21 group (b) or no cell attached to the stroma in control (a) and Zn-1Mg group (c). In the area 2, layers of urothelium are seen as damaged (d, control), thin with 1-3 layers (d, ZM21), and one layer of cuboidal basal cell (f, Zn-1Mg). All urothelium were observed in half from the middle of the section, while another half were similar to area 1. Gradation of layers are nicely presented in area 2 of ZM21 group (e), from no urothelium, single layer, until 3 layers observed from the right side to the left, respectively. In the area 3, complete composition of urothelial cells is clearly seen, and the superficial urothelial cells are distinct in control (g) and Zn-1Mg group (i). Wave-like urothelium was noted in ZM21 group (h), this area is known to be the site of bubbles and thick white structure, it seems obvious that bubbles pushed the urothelium into this shape. Urothelium with clear different urothelial cells were seen in area 4 of control (j), ZM21 group (k) despite the noticeable wave-like structure, and Zn-1Mg group (l). Based on Masson Trichrome staining result, metal alloys groups showed similar morphology compared to controls. Urothelium layers seemed to be normal in all area except under the metal disks.

4.3.3 Histology: Immunofluorescence

Immunostaining analysis from histological section of UE are presented in Figure 16. The differentiated urothelial cells have their role in maintaining the barrier function by producing specific proteins. Immunofluorescence observation was done to assess those proteins. Figure 16 presents the UPK2, ZO-1, Ki67, and laminin-5 immunofluorescence staining on the histological sections of our flat 3D UE model. The absence of native bladder as the positive control in ZO-1, Ki67, and laminin-5 staining was due to the unavailable organ specimen preserved in frozen tissue medium. UPK 2 shows that the uroplakin was not produced on the UE model (Figure 16a-c). ZO-1 staining was done to evaluate the tight junction between urothelial cells. Figure 6f-h shows tight junction between superficial

urothelial cells in each group. This tight junction together with uroplakin play an important role in urothelium, which is known as barrier from urine leakage, ion, or any other compound in the urine. Cell proliferation process on UE model was not observed as shown by the negative result of Ki67 staining (Figure 16i-k). Laminin-5 confirms that delamination or detachment of basal layer did not occurred in both control and metal alloys groups (Figure 16l-n).

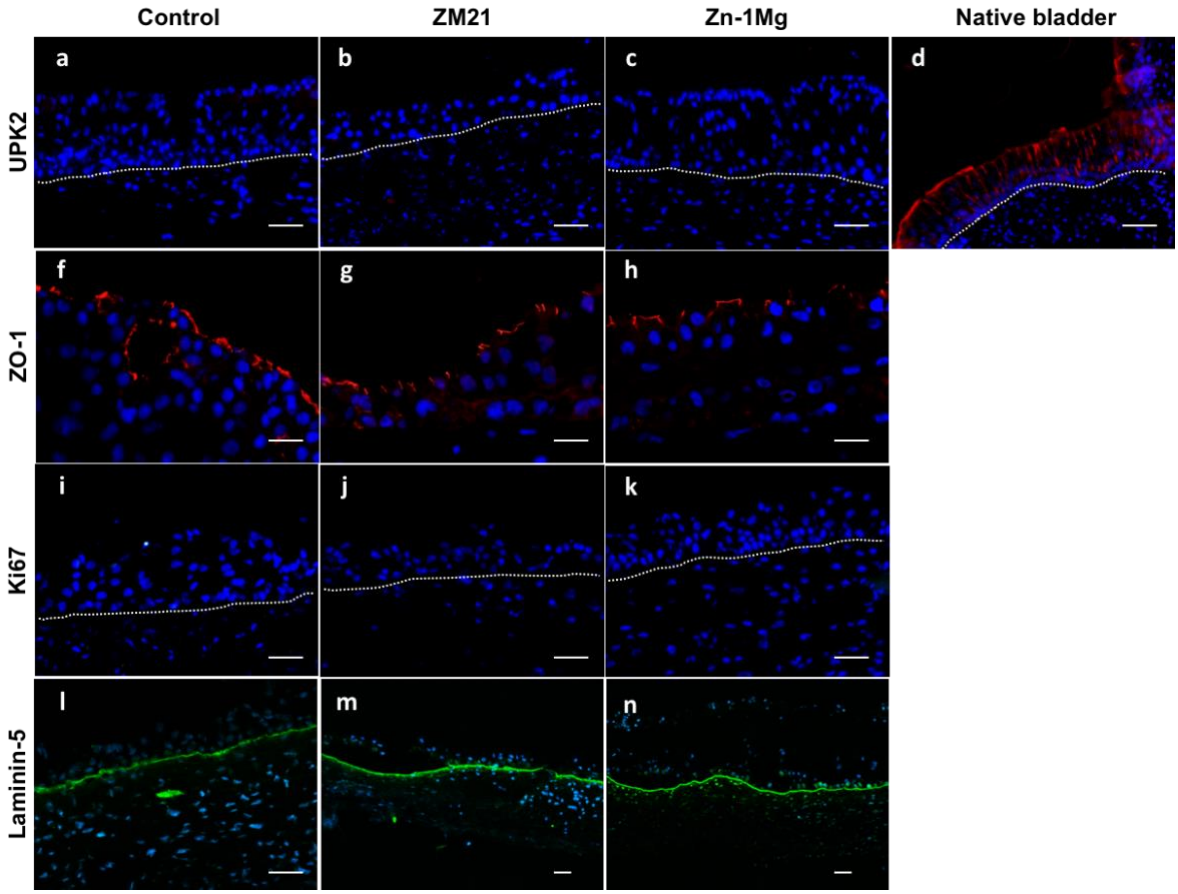

Figure 16 Expression of urothelial differentiation-associated protein and basal lamina in response to contact with metal disk after 7 days of incubation. Immunofluorescence with uroplakin 2 (UPK 2, red) (a-d), anti-ZO-1 (red) (f-h), Ki67 (green) (i-k), and anti-laminin-5 (green) (l-n). Nuclei were stained with Hoechst (blue). Bar=50μm.

Uroplakins protein membrane are specific products of urothelial cells expressed by umbrella cells in the luminal surface [86, 87]. Uroplakins associated with each other and form plaques on the apex of umbrella cells [88]. This protein membrane together with tight

junctions (TJ) between umbrella cells represent the main permeability barrier, as a combination [89]. TJ restricts paracellular diffusion and movement, and it contributes to maintain the surface polarity of the cells by restricting the movement of proteins and lipids between membrane compartments. TJ are composed by cytoplasmic proteins, such as the zonular occludens (ZO) linking TJ to the cytoskeleton, and integral transmembrane proteins, such as occludin, junctional adhesion molecule, and claudins [90-92]. Laminins are a group of proteins that are the most important components of basal membrane. Laminins are expressed in the cytoplasm of basal cells and support the assemble of basal membrane and maintain cell and tissue integrity. It is also involved in cell adhesion, migration, proliferation, differentiation, and preventing programmed cell death. Laminins play role in the interaction between urothelial cells and the extracellular matrix. Laminin-5, one of laminin proteins involved in basal cells adhesion and migration, and hemidesmosomes formation [93-96]. The absence of uroplakin on the surface of the model could be influenced by the compression effect from the metal disks since only the superficial cells produce this specific protein. However, the other 2 important proteins are noted in our flat 3D UE model with direct toxicity method. This means that the urothelium function to produce the barrier proteins was not interrupted by the metals and their degradation products. The urothelium may also still has the permeable barrier function in the close proximity of the cells.

4.4 Scanning electron microscopy

Degradation of metal are noted in alloy groups, while control group showed the same surface as before the incubation (Figure 17). Degradation of ZM21 seen in layers of metal flake all over the surface (d,e), while Zn-1Mg had micro size holes with attached precipitation on some parts of its surface (g,h). Urothelial cells and stroma were observed on the surface of each metal disks (c,f,i). Attachment of cells was marked by the pseudopodia structure in cells with flatten shape. By looking at this result, it was confirmed that the lost or removed part of urothelium from area 1 in UE were actually attached to the metal and got removed together with the metal disks.

The cells that attached were in size of 3-13 μm, indicating that those are basal and intermediate cells [9]. This indicates that the compression on urothelium probably inhibits the urothelial cells to differentiate well. Basal and intermediate cells alone do not have the ability to produce such proteins to maintain the impermeable barrier. Further studies using porous-structured metal sheet to simulate closely the ureteral stent needs to be done.

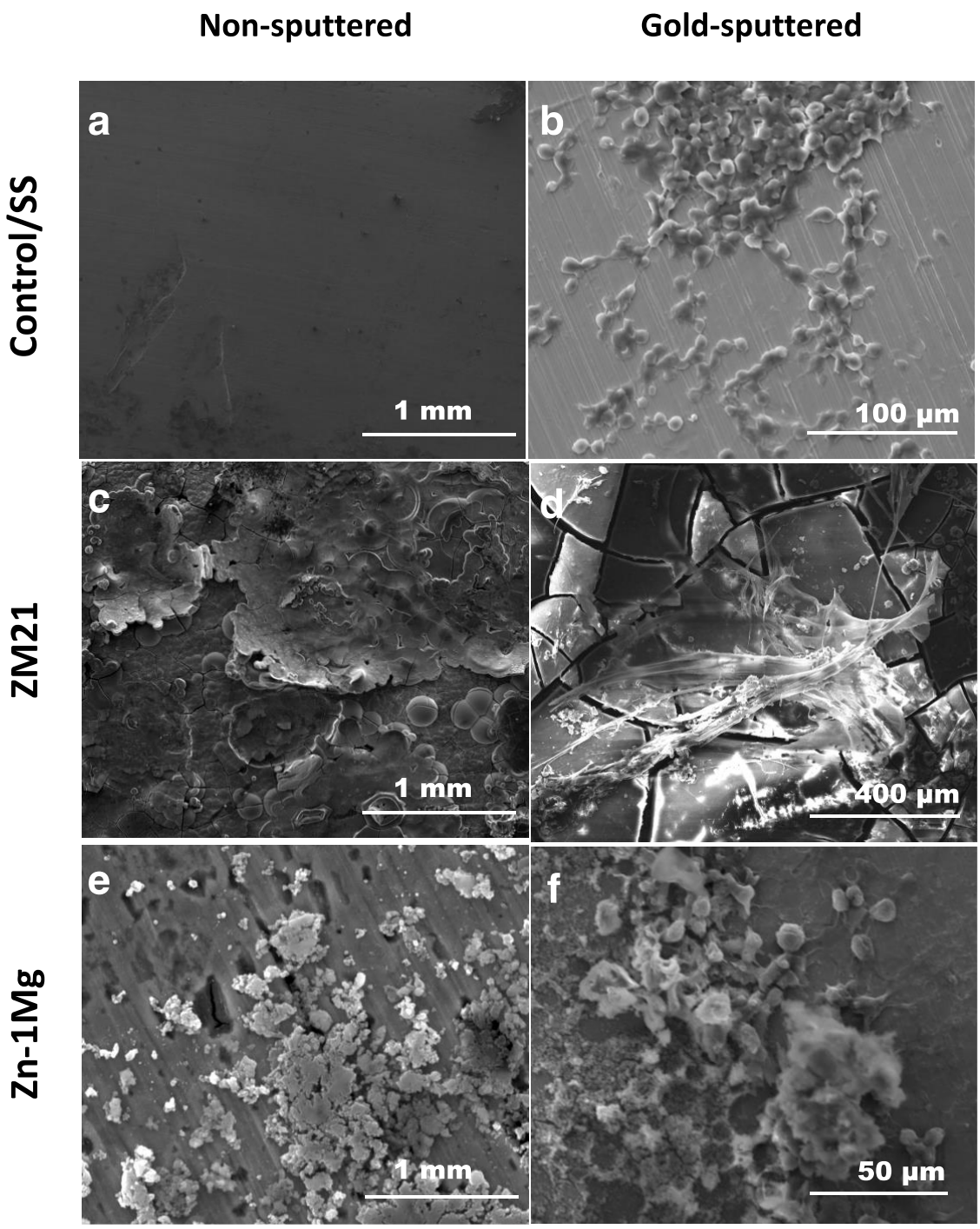

Figure 17 SEM analysis on the surface of metal disks after incubation for 7 days on the top of UEs. Degradation layers were noted on the alloys' surfaces, while controls showed no change (a, c, e). Urothelial cells and stroma collagen layer attachments were observed on the surface of each disks (b, d, f).

Conclusion and Perspective

Conclusion

A study to evaluate the compatibility of biodegradable metals for ureteral stent application was done. The metals used in this study were pure Fe, Mg, and Zn, Mg-2Zn-1Mn, Zn-1Mg, and Zn-0.5Al. The study was done using two series of tests, screening and in-depth evaluation. In the screening step, including preliminary cytotoxicity, electrochemical tests, and IC_{50} estimation, all the metals mentioned before were used and potential metals were selected. Iron was eliminated at the first screening step due to its slow degradation rate and the most toxic toward urothelial cells. At the second step, i.e. IC_{50} estimation, it is revealed that Mg has a narrow range of safe concentration. Therefore, it was eliminated.

In-depth testing was done by cytotoxicity test conducted on both monolayer culture of urothelial cells and flat 3D tissue-engineered ureteral wall models. Monolayer indirect cytotoxicity test was done to observe the cell health with the presence of biodegradable metal ions. The ureteral wall model was tested with direct contact with the metal disks and the cell functions were observed in the presence of degrading metals and their degradation product, as well as the compression from the weight of metal disks. The results showed that a survival mode was observed on urothelial cells as a respond to the toxicity of metal extracts in monolayer culture. High pH value of metal extracts had a significant contribution to lower cell viability. The cytokeratin observation showed a significant proof of cell stress that lead to apoptosis.

The result of direct toxicity tests on flat 3D culture by Masson Trichrome staining showed the morphological changes of urothelium to respond the metal and its corrosion as toxic agents. It showed that metals have effect on the morphology of cell layers, while urothelium was still able to maintain its function to produce the barrier protein and may have the permeable barrier function in the close proximity of the cells. This indicates that the tissue is healthy with the presence of metal disks and their degradation products after 7 days. The attached cell layers on the surface of metal disks may indicate that the metal specimens are non-toxic. It could be predicted that the wound or lesion of the metal compression will heal completely with relatively short time after the compression is

removed. Direct toxicity test also showed that the 3D structure with differentiated urothelial layers gives stable model for in-vitro testing.

Perspective

Zinc-based biodegradable metals, which in this study were Zn-1Mg and Zn-0.5Al are the promising candidates for ureteral stent application based on the results shown in this study. More in-depth tests should be done to confirm. The evaluation of cell apoptosis should be continued in term of both stages and pathway also to distinguish between apoptosis and necrosis in the presence of metal ions. The apoptosis stages and necrosis determination can be done by using Annexin/PI test in flowcytometer, while cell death pathway by Western Immunoblotting. Comet assay is also useful to evaluate the metals potential genotoxic effect toward urothelial cells.

Direct toxicity test on flat 3D tissue with mesh-like structure metals can be conducted to follow up this study. The use of mesh-like structure metal samples is expected to give the similar condition with the US currently use in clinical application. The results that could be expected are the normal differentiation of UC into urothelium under the metal in the presence of air provided by porous structure samples. A permeability test to confirm the barrier function of urothelium can be done following the direct toxicity test.

3D ureteral tissue-engineered with a tubular shape and with bioreactor system could follow the flat 3D direct toxicity step. This test aims to have a close simulation of urinary condition with the use of controlled aU solution flow inside the lumen of engineered ureteral tissue and metal samples in ring shape to model the common US available. The results that could be expected from this test are the degradation behavior of metal samples and their effect on ureteral tissue in a close simulated urinary environment.

After the cytotoxicity assessment done and the toxicity of biodegradable metals used in this work are confirmed, the evaluation of the antibacterial activity of the metals and

encrustation ability in aU solution could follow. The expected results are the determination of metals' antibacterial effectiveness and encrustation ability.

BIBLIOGRAPHY

[1] Frazier MS. Essentials of human diseases and conditions. 3rd ed ed. St. Louis, MO: Elsevier Saunders; 2004.

[2] Hall JE. Guyton and Hall Textbook of Medical Physiology: Elsevier Health Sciences; 2010.

[3] Wattis JAD, Oliver JM, Grant DM, Cummings LJ, Bishop M, Bayston R, et al. Ureteric stents: investigating flow and encrustation. Proceedings of the Institution of Mechanical Engineers, Part H: Journal of Engineering in Medicine 2008;222:551-61.

[4] Gulmi FA, Felsen D. Pathophysiology of Urinary Tract Obstruction. Smith's Textbook of Endourology: Wiley-Blackwell; 2012. p. 95-119.

[5] Linton KD, Hall J. Obstruction of the upper and lower urinary tract. Surgery (Oxford) 2013;31:346-53.

[6] Yi JH, Shin HJ, Kim SM, Han SW, Kim HJ, Oh MS. Does the exposure of urine samples to air affect diagnostic tests for urine acidification? Clin J Am Soc Nephrol 2012;7:1211-6.

[7] Yaroshenko I, Kirsanov D, Kartsova L, Sidorova A, Borisova I, Legin A. Determination of urine ionic composition with potentiometric multisensor system. Talanta 2015;131:556-61.

[8] Putnam DF, Company-West MDA, Center LR, Aeronautics USN, Administration S. Composition and Concentrative Properties of Human Urine: National Aeronautics and Space Administration; 1971.

[9] Khandelwal P, Abraham SN, Apodaca G. Cell biology and physiology of the uroepithelium. Am J Physiol Renal Physiol 2009;297:F1477-501.

[10] Chapple CR, Steers WD. Practical Urology: Essential Principles and Practice: Essential Principles and Practice: Springer London; 2011.

[11] Mescher A. Junqueira's Basic Histology: Text and Atlas, 12th Edition: McGraw-Hill Education; 2009.

[12] Chevalier RL. Chapter 19 - Obstructive Uropathy: Assessment of Renal Function in the Fetus A2 - Oh, William. In: Guignard J-P, Baumgart S, editors. Nephrology and Fluid/Electrolyte Physiology: Neonatology Questions and Controversies (Second Edition). Philadelphia: W.B. Saunders; 2012. p. 335-59.

[13] Reyner K, Heffner AC, Karvetski CH. Urinary obstruction is an important complicating factor in patients with septic shock due to urinary infection. The American Journal of Emergency Medicine 2015.

[14] J. Mickelson, UPJ obstruction. 2013. http://www.metrovanurology.com/content/upj-obstruction.

[15] Borin JF, McDougall EM. Ureteral Stent for Ureteral Stricture. In: Baba S, Ono Y, editors. Interventional Management of Urological Diseases. Tokyo: Springer Japan; 2006. p. 75-86.

[16] Lock JY, Wyatt E, Upadhyayula S, Whall A, Nunez V, Vullev VI, et al. Degradation and antibacterial properties of magnesium alloys in artificial urine for potential resorbable ureteral stent applications. J Biomed Mater Res A 2014;102:781-92.

[17] ASTM F1828-17, Standard Specification for Ureteral Stents, ASTM International, West Conshohocken, PA, 2017, www.astm.org

[18] Brotherhood H, Lange D, Chew BH. Advances in ureteral stents. Transl Androl Urol 2014;3:314-9.

[19] Lange D, Bidnur S, Hoag N, Chew BH. Ureteral stent-associated complications--where we are and where we are going. Nat Rev Urol 2015;12:17-25.
[20] Yang L, Whiteside S, Cadieux PA, Denstedt JD. Ureteral stent technology: Drug-eluting stents and stent coatings. Asian Journal of Urology 2015;2:194-201.
[21] Lange D, Elwood CN, Choi K, Hendlin K, Monga M, Chew BH. Uropathogen interaction with the surface of urological stents using different surface properties. J Urol 2009;182:1194-200.
[22] Wang R, Neoh KG, Kang ET, Tambyah PA, Chiong E. Antifouling coating with controllable and sustained silver release for long-term inhibition of infection and encrustation in urinary catheters. J Biomed Mater Res B Appl Biomater 2015;103:519-28.
[23] Jose Ruben Morones-Ramirez JAW, Catherine S. Spina, James J. Collins. Silver enhances antibiotic activity against gram-negative bacteria. Science Translational Medicine 2013;5:1-11.
[24] Wakshlak RB, Pedahzur R, Avnir D. Antibacterial activity of silver-killed bacteria: the "zombies" effect. Sci Rep 2015;5:9555.
[25] Chew BH, Lange D, Paterson RF, Hendlin K, Monga M, Clinkscales KW, et al. Next generation biodegradable ureteral stent in a yucatan pig model. J Urol 2010;183:765-71.
[26] Chew BH, Paterson RF, Clinkscales KW, Levine BS, Shalaby SW, Lange D. In vivo evaluation of the third generation biodegradable stent: a novel approach to avoiding the forgotten stent syndrome. J Urol 2013;189:719-25.
[27] Zou T, Wang L, Li W, Wang W, Chen F, King MW. A resorbable bicomponent braided ureteral stent with improved mechanical performance. J Mech Behav Biomed Mater 2014;38:17-25.
[28] Hadaschik BA, Paterson RF, Fazli L, Clinkscales KW, Shalaby SW, Chew BH. Investigation of a novel degradable ureteral stent in a porcine model. J Urol 2008;180:1161-6.
[29] Wang X, Shan H, Wang J, Hou Y, Ding J, Chen Q, et al. Characterization of nanostructured ureteral stent with gradient degradation in a porcine model. Int J Nanomedicine 2015;10:3055-64.
[30] Hamad K, Kaseem M, Yang HW, Deri F, Ko YG. Properties and medical applications of polylactic acid: A review. Express Polymer Letters 2015;9:435-55.
[31] Chew BH, Lange D. Ureteral stent symptoms and associated infections: a biomaterials perspective. Nat Rev Urol 2009;6:440-8.
[32] Zhang S, Zheng Y, Zhang L, Bi Y, Li J, Liu J, et al. In vitro and in vivo corrosion and histocompatibility of pure Mg and a Mg-6Zn alloy as urinary implants in rat model. Mater Sci Eng C Mater Biol Appl 2016;68:414-22.
[33] Mahyudin F, Hermawan H. Biomaterials and Medical Devices: A Perspective from an Emerging Country: Springer International Publishing; 2016.
[34] Zheng YF, Gu XN, Witte F. Biodegradable metals. Materials Science and Engineering: R: Reports 2014;77:1-34.
[35] Murni NS, Dambatta MS, Yeap SK, Froemming GR, Hermawan H. Cytotoxicity evaluation of biodegradable Zn-3Mg alloy toward normal human osteoblast cells. Mater Sci Eng C Mater Biol Appl 2015;49:560-6.
[36] Kubásek J, Vojtěch D, Jablonská E, Pospíšilová I, Lipov J, Ruml T. Structure, mechanical characteristics and in vitro degradation, cytotoxicity, genotoxicity and

mutagenicity of novel biodegradable Zn–Mg alloys. Materials Science and Engineering: C 2016;58:24-35.
[37] Bowen PK, Drelich J, Goldman J. Zinc exhibits ideal physiological corrosion behavior for bioabsorbable stents. Adv Mater 2013;25:2577-82.
[38] Bowen PK, Guillory RJ, 2nd, Shearier ER, Seitz JM, Drelich J, Bocks M, et al. Metallic zinc exhibits optimal biocompatibility for bioabsorbable endovascular stents. Mater Sci Eng C Mater Biol Appl 2015;56:467-72.
[39] Frassinetti S, Bronzetti G, Caltavuturo L, Cini M, Croce CD. The role of zinc in life: a review. Journal of environmental pathology, toxicology and oncology : official organ of the International Society for Environmental Toxicology and Cancer 2006;25:597-610.
[40] David R. Antimicrobials: Why zinc is bad for bacteria. Nat Rev Micro 2012;10:4-.
[41] Xie Y, He Y, Irwin PL, Jin T, Shi X. Antibacterial activity and mechanism of action of zinc oxide nanoparticles against Campylobacter jejuni. Appl Environ Microbiol 2011;77:2325-31.
[42] Pasquet J, Chevalier Y, Pelletier J, Couval E, Bouvier D, Bolzinger M-A. The contribution of zinc ions to the antimicrobial activity of zinc oxide. Colloids and Surfaces A: Physicochemical and Engineering Aspects 2014;457:263-74.
[43] Frederick S, Begley TP. Biocompatibility of Materials in Medical Devices. Wiley Encyclopedia of Chemical Biology: John Wiley & Sons, Inc.; 2007.
[44] Saliterman S. Fundamentals of BioMEMS and Medical Microdevices: Wiley; 2006.
[45] Ducheyne P, Healy K, Hutmacher DE, Grainger DW, Kirkpatrick CJ. Comprehensive Biomaterials: Elsevier Science; 2015.
[46] Ratner BD, Hoffmann AS, Schoen FJ, Lemons JE. Biomaterials Science- An Introduction to Materials in Medicine. 2nd ed. China: Elsevier Academic Press; 2004.
[47] Amato SF. 4 - Clinical development and endpoint strategies for biomaterials and medical devices. Regulatory Affairs for Biomaterials and Medical Devices: Woodhead Publishing; 2015. p. 47-66.
[48] Yang L, Zhang E. Biocorrosion behavior of magnesium alloy in different simulated fluids for biomedical application. Materials Science and Engineering: C 2009;29:1691-6.
[49] Borenfreund E, Puerner JA. Toxicity determined in vitro by morphological alterations and neutral red absorption. Toxicol Lett 1985;24:119-24.
[50] Franken NA, Rodermond HM, Stap J, Haveman J, van Bree C. Clonogenic assay of cells in vitro. Nat Protoc 2006;1:2315-9.
[51] Germain L, Rouabhia M, Guignard R, Carrier L, Bouvard V, Auger FA. Improvement of human keratinocyte isolation and culture using thermolysin. Burns 1993;19:99-104.
[52] Dee KC, Puleo DA, Bizios R. An Introduction to Tissue-Biomaterial Interactions: Wiley; 2003.
[53] Hollinger JO. An Introduction to Biomaterials, Second Edition: CRC Press; 2011.
[54] Mostaed E, Sikora-Jasinska M, Mostaed A, Loffredo S, Demir AG, Previtali B, et al. Novel Zn-based alloys for biodegradable stent applications: Design, development and in vitro degradation. J Mech Behav Biomed Mater 2016;60:581-602.
[55] ASTM International. *ASTM F2129-17 Standard Test Method for Conducting Cyclic Potentiodynamic Polarization Measurements to Determine the Corrosion Susceptibility of Small Implant Devices*; ASTM International: West Conshohocken, PA, USA, 2017.

[56] Magnan M, Lévesque P, Gauvin R, Dubé J, Barrieras D, El-Hakim A, et al. Tissue engineering of a genitourinary tubular tissue graft resistant to suturing and high internal pressures. Tissue engineering Part A 2008;15:197-202.
[57] Chabaud S, Saba I, Baratange C, Boiroux B, Leclerc M, Rousseau A, et al. Urothelial cell expansion and differentiation are improved by exposure to hypoxia. J Tissue Eng Regen Med 2017.
[58] Freshney RI. Culture of Animal Cells: A Manual of Basic Technique and Specialized Applications: Wiley; 2011.
[59] Imbeault A, Bernard G, Rousseau A, Morissette A, Chabaud S, Bouhout S, et al. An endothelialized urothelial cell-seeded tubular graft for urethral replacement. Can Urol Assoc J 2013;7:E4-9.
[60] Cattan V, Bernard G, Rousseau A, Bouhout S, Chabaud S, Auger FA, et al. Mechanical stimuli-induced urothelial differentiation in a human tissue-engineered tubular genitourinary graft. Eur Urol 2011;60:1291-8.
[61] Bouhout S, Perron É, Gauvin R, Bernard G, Ouellet G, Cattan V, et al. In vitro reconstruction of an autologous, watertight, and resistant vesical equivalent. Tissue Engineering Part A 2010;16:1539-48.
[62] Heckman C, Kanagasundaram S, Cayer M, Paige J. Preparation of cultured cells for scanning electron microscope. 2007.
[63] Lienemann CP, Dreyfus S, Pecheyran C, Donard OFXJO, Science G, IFP T-R. Trace Metal Analysis in Petroleum Products: Sample Introduction Evaluation in ICP-OES and Comparison with an ICP-MS Approach. 2007;62:69-77.
[64] Şahan Y, Basoglu F, Gücer S. ICP-MS analysis of a series of metals (Namely: Mg, Cr, Co, Ni, Fe, Cu, Zn, Sn, Cd and Pb) in black and green olive samples from Bursa, Turkey. Food Chemistry 2007;105:395-9.
[65] Goullé J-P, Mahieu L, Castermant J, Neveu N, Bonneau L, Lainé G, et al. Metal and metalloid multi-elementary ICP-MS validation in whole blood, plasma, urine and hair: Reference values. Forensic Science International 2005;153:39-44.
[66] Zhang XL, Jiang ZH, Yao ZP, Song Y, Wu ZD. Effects of scan rate on the potentiodynamic polarization curve obtained to determine the Tafel slopes and corrosion current density. Corrosion Science 2009;51:581-7.
[67] Witte F, Eliezer A. Biodegradable Metals. In: Eliaz N, editor. Degradation of Implant Materials. New York, NY: Springer New York; 2012. p. 93-109.
[68] Witecka A, Bogucka A, Yamamoto A, Mathis K, Krajnak T, Jaroszewicz J, et al. In vitro degradation of ZM21 magnesium alloy in simulated body fluids. Mater Sci Eng C Mater Biol Appl 2016;65:59-69.
[69] Tian Q, Deo M, Rivera-Castaneda L, Liu H. Cytocompatibility of Magnesium Alloys with Human Urothelial Cells: A Comparison of Three Culture Methodologies. ACS Biomaterials Science & Engineering 2016;2:1559-71.
[70] Champagne S, Mostaed E, Safizadeh F, Ghali E, Vedani M, Hermawan H. In Vitro Degradation of Absorbable Zinc Alloys in Artificial Urine. Materials (Basel) 2019;12.
[71] Kubasek J, Vojtech D, Jablonska E, Pospisilova I, Lipov J, Ruml T. Structure, mechanical characteristics and in vitro degradation, cytotoxicity, genotoxicity and mutagenicity of novel biodegradable Zn-Mg alloys. Mater Sci Eng C Mater Biol Appl 2016;58:24-35.

[72] Murni N, Dambatta M, Yeap S, Froemming G, Hermawan H. Cytotoxicity evaluation of biodegradable Zn–3Mg alloy toward normal human osteoblast cells. Materials Science and Engineering: C 2015;49:560-6.
[73] Shen C, Liu X, Fan B, Lan P, Zhou F, Li X, et al. Mechanical properties, in vitro degradation behavior, hemocompatibility and cytotoxicity evaluation of Zn-1.2Mg alloy for biodegradable implants. RSC Advances 2016;6:86410-9.
[74] Dambatta MS, Murni NS, Izman S, Kurniawan D, Froemming GR, Hermawan H. In vitro degradation and cell viability assessment of Zn-3Mg alloy for biodegradable bone implants. Proc Inst Mech Eng H 2015;229:335-42.
[75] Kruse CR, Singh M, Targosinski S, Sinha I, Sorensen JA, Eriksson E, et al. The effect of pH on cell viability, cell migration, cell proliferation, wound closure, and wound reepithelialization: In vitro and in vivo study. Wound Repair Regen 2017;25:260-9.
[76] Gu X, Wang F, Xie X, Zheng M, Li P, Zheng Y, et al. In vitro and in vivo studies on as-extruded Mg- 5.25wt.%Zn-0.6wt.%Ca alloy as biodegradable metal. Science China Materials 2018;61:619-28.
[77] Galow A-M, Rebl A, Koczan D, Bonk SM, Baumann W, Gimsa J. Increased osteoblast viability at alkaline pH in vitro provides a new perspective on bone regeneration. Biochemistry and Biophysics Reports 2017;10:17-25.
[78] Alguacil J, Kogevinas M, Silverman DT, Malats N, Real FX, Garcia-Closas M, et al. Urinary pH, cigarette smoking and bladder cancer risk. Carcinogenesis 2011;32:843-7.
[79] Bourdeau P, Environment ICoSUSCoPot. Short-term toxicity tests for non-genotoxic effects: Wiley; 1990.
[80] Hsiao IL, Huang YJ. Effects of serum on cytotoxicity of nano- and micro-sized ZnO particles. J Nanopart Res 2013;15:1829.
[81] Hiebl B, Peters S, Gemeinhardt O, Niehues SM, Jung F. Impact of serum in cell culture media on in vitro lactate dehydrogenase (LDH) release determination. Journal of Cellular Biotechnology 2017;3:9-13.
[82] Sumitran-Holgersson PCaS. Cytokeratins of the Liver and Intestine Epithelial Cells During Development and Disease. In: Hamilton G, editor. Cytokeratins - Tools in Oncology: InTech; 2012. p. 15-32.
[83] Ku NO, Toivola DM, Strnad P, Omary MB. Cytoskeletal keratin glycosylation protects epithelial tissue from injury. Nat Cell Biol 2010;12:876-85.
[84] Karantza V. Keratins in health and cancer: more than mere epithelial cell markers. Oncogene 2011;30:127-38.
[85] Birder L, Andersson KE. Urothelial signaling. Physiol Rev 2013;93:653-80.
[86] Wu XR, Kong XP, Pellicer A, Kreibich G, Sun TT. Uroplakins in urothelial biology, function, and disease. Kidney Int 2009;75:1153-65.
[87] Kaufmann O, Volmerig J, Dietel M. Uroplakin III is a highly specific and moderately sensitive immunohistochemical marker for primary and metastatic urothelial carcinomas. American journal of clinical pathology 2000;113:683-7.
[88] Jenkins D, Woolf AS. Uroplakins: new molecular players in the biology of urinary tract malformations. Kidney Int 2007;71:195-200.
[89] Hu P, Meyers S, Liang F-X, Deng F-M, Kachar B, Zeidel ML, et al. Role of membrane proteins in permeability barrier function: uroplakin ablation elevates urothelial permeability. American Journal of Physiology - Renal Physiology 2002;283:F1200-F7.

[90] Varley CL, Garthwaite MA, Cross W, Hinley J, Trejdosiewicz LK, Southgate J. PPARγ-Regulated Tight Junction Development During Human Urothelial Cytodifferentiation. Journal of cellular physiology 2006;208:407-17.
[91] Smith NJ, Hinley J, Varley CL, Eardley I, Trejdosiewicz LK, Southgate J. The human urothelial tight junction: claudin 3 and the ZO-1alpha+ switch. Bladder (San Franc) 2015;2:e9.
[92] Rickard A, Dorokhov N, Ryerse J, Klumpp DJ, McHowat J. Characterization of tight junction proteins in cultured human urothelial cells. In Vitro Cell Dev Biol Anim 2008;44:261-7.
[93] Brunner A, Tzankov A. The Role of Structural Extracellular Matrix Proteins in Urothelial Bladder Cancer (Review). Biomarker Insights 2007;2:418-27.
[94] Florea F, Koch M, Hashimoto T, Sitaru C. Autoimmunity against laminins. Clin Immunol 2016;170:39-52.
[95] Hattori K, Mabuchi R, Fujiwara H, Sanzen N, Sekiguchi K, Kawai K, et al. Laminin expression patterns in human ureteral tissue. J Urol 2003;170:2040-3.
[96] Southgate J, Harnden P, Selby PJ, Thomas DFM, Trejdosiewicz LK. Urothelial Tissue Regulation. In: Baskin LS, Hayward SW, editors. Advances in Bladder Research. Boston, MA: Springer US; 1999. p. 19-30.